ANNUAL REVIEWS

Annual Review of Marine Science

Changing Tides: The Role of Natural and Anthropogenic Factors

Stefan A. Talke[1] and David A. Jay[2]

[1]Department of Civil and Environmental Engineering, California Polytechnic State University, San Luis Obispo, California 94307, USA; email: stalke@calpoly.edu

[2]Department of Civil and Environmental Engineering, Portland State University, Portland, Oregon 97207, USA

Annu. Rev. Mar. Sci. 2020. 12:121–51

First published as a Review in Advance on September 3, 2019

The *Annual Review of Marine Science* is online at marine.annualreviews.org

https://doi.org/10.1146/annurev-marine-010419-010727

Keywords

tides, storm surge, sea-level rise, anthropogenic effects, estuaries, tidal rivers

Abstract

Tides are changing worldwide at rates not explained by astronomical forcing. Rather, the observed evolution of tides and other long waves, such as storm surges, is influenced by shelf processes and changes to the roughness, depth, width, and length of embayments, estuaries, and tidal rivers. In this review, we focus on processes in estuaries and tidal rivers, because that is where the largest changes to tidal properties are occurring. Recent literature shows that changes in tidal amplitude have been ubiquitous worldwide over the past century, often in response to wetland reclamation, channel dredging, and other environmental changes. While tidal amplitude changes are sometimes slight (<1%) or even negative, we identify two types of systems that are particularly prone to tidal amplification: (*a*) shallow, strongly damped systems, in which a small increase in depth produces a large decrease in effective friction, and (*b*) systems in which wave reflection and resonance are strongly influenced by changes to depth, friction, and convergence. The largest changes in amplitude occur inland, some distance from the coast, and can sometimes be measured in meters. Tide changes are a leading indicator that the dynamics of storm surges and river flood waves have also changed and are often associated with shifts in sediment transport, salinity intrusion, and ecosystem properties. Therefore, the dynamics of tidal evolution have major implications for coastal management, particularly for systems that are sensitive to changes in geometry induced by sea-level rise and anthropogenic development.

INTRODUCTION

Relative sea-level rise: the local rate at which annually averaged water levels are changing relative to nearby land

Relative sea-level rise is increasing flood hazard worldwide (Bilskie et al. 2014, Neumann et al. 2015). Over the past few decades, a rising sea-level baseline has in many regions led to sharp increases in nuisance or sunny-day flooding, in which a large predicted tide—often augmented by local winds—exceeds natural and constructed barriers (Sweet & Park 2014, Moftakhari et al. 2015). As sea level rises, storm tides—a combination of tides and a meteorologically formed long wave—will increasingly inundate coastal regions and impact human populations (e.g., Hinkel et al. 2014, Neumann et al. 2015). A simple approach to assess altered flood risk is to raise existing hazard curves by the expected local sea-level rise. However, tidal records, theory, and numerical models all suggest that depth and width changes induced by sea-level rise feed back into coastal tide, surge, and wind-wave magnitudes in a nonlinear manner (e.g., Holleman & Stacey 2014, Arns et al. 2017). The purpose of this review is to assess the sensitivity of tides to changes in the geometry of bays, estuaries, and rivers caused by sea-level rise, anthropogenic activity, and other environmental changes.

Water depth exerts a strong influence on tides. The proportional change in depth caused by sea-level rise will be largest in shallow systems, as long as the relative sea-level rise exceeds the sedimentation rate. Recent probabilistic assessments suggest a global sea-level rise of 0.3–1.3 m by 2100, though high-end scenarios suggest a rise of 2–2.5 m (Sweet et al. 2017 and references therein), much larger than the historical rise of approximately 0.14–0.19 m during the twentieth century (Church & White 2011, Hay et al. 2015). Nonetheless, relative rise rates vary greatly. Within the United States, relative sea level is falling in some regions, such as Alaska (e.g., −0.96 mm/y in Anchorage), and rising rapidly along the Gulf Coast and southeast coast due to land subsidence (e.g., +6.5 mm/y in Galveston, Texas). These variations in relative sea-level trends are caused by differential changes in ocean sea level resulting from ice melt, thermal expansion, oceanic water redistribution, changing ocean currents, and gravitational fingerprinting, and by spatial variations in vertical land motion resulting from processes such as glacial isostatic adjustment, plate tectonics, and compaction (Syvitski et al. 2009, Nicholls & Cazenave 2010, Hay et al. 2015). The land around many cities is subsiding quickly due to groundwater extraction, particularly in Southeast Asia (e.g., Jakarta and Manila), greatly exacerbating flood risk (Nicholls & Cazenave 2010, Hallegatte et al. 2013). Moreover, many regions experience significant interannual, seasonal, and decadal fluctuations in sea level (Zhang & Church 2012). These sea-level fluctuations are often correlated with variations in tidal properties (Devlin et al. 2014).

A different type of depth change is also ubiquitous within estuaries and provides clues to the dynamic changes that sea-level rise might cause. Over time, anthropogenic activity has completely reworked the underwater landscape of major estuaries and deltaic regions (e.g., Syvitski et al. 2009, Chant et al. 2018). Historically, multiple harbors and estuaries silted up due to increased sediment load caused by agricultural, mining, or industrial practices (e.g., Gilbert 1917, Montgomery 2007). More recently, sediment supply to some rivers has been limited by the construction of reservoirs, potentially leading to erosion (Naik & Jay 2011, Schoellhamer 2011, Templeton & Jay 2013) and influencing wetland and deltaic bathymetry (Syvitski et al. 2009). The increasing size of ships since the late nineteenth century has led to straightening (streamlining) and dredging of shipping channels (de Jonge et al. 2014, Chant et al. 2018, Ralston et al. 2019), with the controlling depth now often more than double predevelopment depths (Familkhalili & Talke 2016). Wetland reclamation for human use has occurred throughout history (van de Ven 1993, Seasholes 2003), and rapid coastal wetland loss continues, for example, on the US Gulf and East Coasts (Dahl & Stedman 2013) and within Southeast Asia (Murray et al. 2014). Because dredging and filling are driven by global economic development, the anthropogenic footprint on local estuarine bathymetry is worldwide. Hence, to the extent that tide gauge measurements coincide with human-induced bathymetric change, we have a natural experiment in which data can help us understand how tidal dynamics are perturbed under changing conditions. Future sea-level rise will likely result in continued wetland loss (Nicholls et al. 1999) and depth changes.

The importance of any anthropogenic effect on tidal properties must be placed in context with the natural, astronomically induced variations in tides caused by the orbital motions of the moon, sun, and earth (e.g., Doodson 1921, Cartwright & Tayler 1971, Pugh 1987). These variations produce daily, monthly, annual, 8.85-year, nodal (18.61-year), and longer-term patterns in tidal amplitudes and are typically represented as a sum of sinusoidal waves, each with a different amplitude, phase, and frequency (e.g., Doodson 1921, Foreman 1977, Godin 1986, Foreman & Henry 1989). In most locations, the largest constituent sine wave is M_2 (~12.42-h period), which produces tides that occur approximately twice a day. Other major semidiurnal constituents include S_2 (12-h period) and N_2 (~12.65-h period). Significant tidal energy also occurs in the diurnal band (once daily), with the largest constituents in the band being K_1 (~23.93-h period) and O_1 (25.82-h period). Some regions, such as the North Atlantic, are dominated by semidiurnal tides, while others, such as the Gulf of Mexico, have predominantly diurnal tides. Regions with significant semidiurnal and diurnal constituents are marked by a diurnal inequality, i.e., one large and one small tide a day. In shallow water, frictional processes extract energy from astronomically forced constituents and transfer energy to both higher and lower frequencies. Notable examples of such shallow-water constituents (also called overtides) occur at frequencies of four and six times a day (Godin 1986). The details of the energy transfer to overtides often provide clues as to how and why tidal amplitudes are changing (Parker 1991, Chernetsky et al. 2010, Devlin et al. 2014). Pugh (1987, and references therein) provided a full description of important constituents and their origins, and the IHO (1994) provided a glossary of terms used in tidal science.

The summation of multiple sine waves produces interesting cycles and beat patterns. An approximately two-week-long spring tide–neap tide cycle in tidal range is produced by the superposition of the M_2 and S_2 constituents (~14.8-day period) and/or the K_1 and O_1 constituents (~13.7-day period) (Kvale 2006). In regions with mixed semidiurnal and diurnal tides, such as the US West Coast, both diurnal and semidiurnal spring–neap cycles are present and slowly move into and out of phase with each other, producing seasonal variations in tidal amplitudes and the diurnal inequality. Also, adding N_2 to a time series of M_2 and S_2 produces one large and one small spring–neap period each month. Additional constituents add together to produce further seasonal, annual, and longer-term variability. There are hundreds of small, minor constituents, many of which are not resolvable in tide data sets because they (*a*) are in the noise floor of the measurement and/or (*b*) are satellites of the major constituents and are so close in frequency that they cannot be resolved (Cartwright & Tayler 1971, Godin 1986). Some satellite constituents modulate M_2 and K_1 by 3.73% and 11.58%, respectively, over an 18.61-year nodal cycle (Cartwright & Tayler 1971); a list of other constituent modulations was given by Pugh (1987). In coastal regions, friction reduces this 18.61-year modulation (Godin 1986, Ray & Talke 2019). A smaller, difficult-to-resolve, 8.85-year modulation also occurs. One implication of the nodal cycle and the many constituents is that any assessment of changing tides must account for such natural variability; in practice, this means that long time series (>30–50 years; Jay 2009, Woodworth 2010) are generally required to quantify nonastronomical trends.

In addition to astronomical forcing, many environmental and geophysical factors influence tidal amplitudes (**Figure 1**). Environmental changes that can influence tides in estuaries and coastal bays include (*a*) changes to depth, width, and length caused by relative sea-level rise, dredging, and land reclamation; (*b*) changes to mixing dynamics and energy dissipation caused by altered stratification, bed roughness, or nonlinear interaction with other forcing factors,

Semidiurnal constituent: a tidal component that has a period near 12 h; a subscript 2 denotes that it occurs approximately twice a day

Diurnal constituent: a tidal component of the tide with a period near 24 h; a subscript 1 denotes that it occurs approximately once a day

Shallow-water constituent (overtide): a tidal constituent produced by nonlinear interactions (e.g., friction) in shallow water; the subscript denotes the number of times a day the wave occurs

Spring tide: the time period every two weeks when the tidal range is much larger than usual

Neap tide: the time period every two weeks when the tidal range is much smaller than usual

Tidal range: the difference between the average of twice-daily high water and average of twice-daily low water

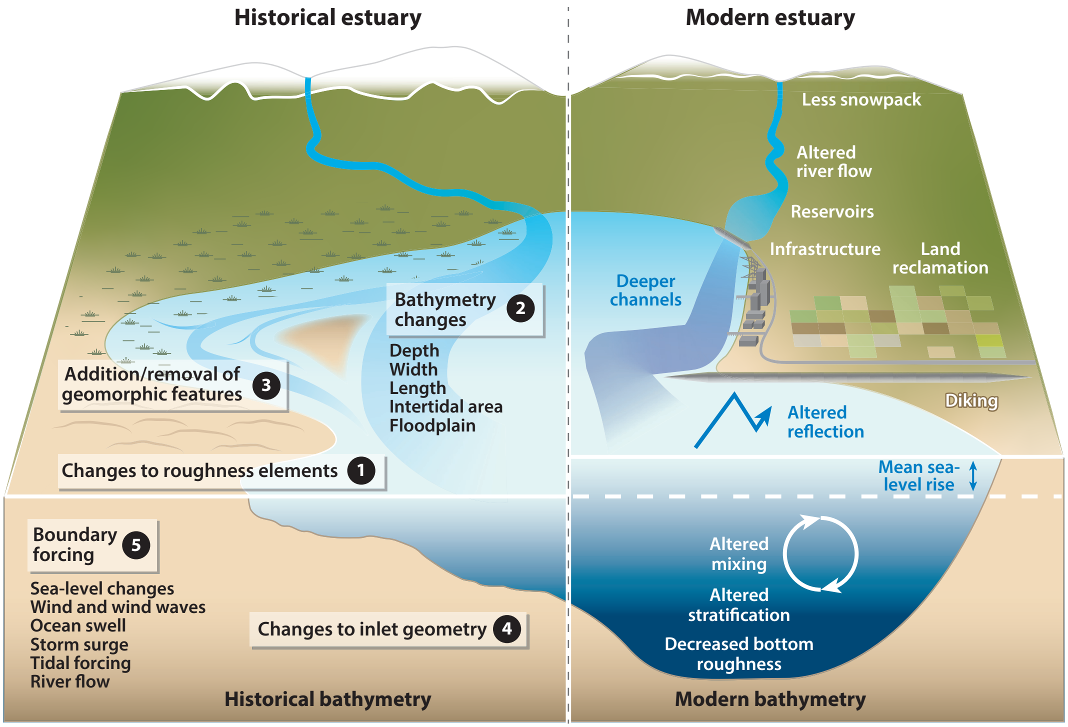

Figure 1

Schematic of factors within rivers, estuaries, and coastal embayments that can produce an evolution in tidal properties. Any significant bathymetric change potentially affects tides, particularly when the change is large scale. (❶) At the bed, changes to roughness elements (e.g., dunes, bed material, wetland plants, or infrastructure) alter frictional drag. (❷) Altered bathymetry (e.g., depth) caused by dredging, scouring, sediment deposition, or sea-level rise influences tidal damping. (❸) The removal or addition of flood plains, wetland areas, islands, intertidal flats, and subtidal flats affects the tidal prism and dissipation. (❹) Changing inlet geometry can produce substantial effects, as can the introduction of reflective boundaries (e.g., infrastructure). (❺) Boundary forcing also matters: Changes to river discharge caused by flow regulation, diversion, and climate change affect seasonal tidal patterns and long-term trends. Alterations in wind, waves, stratification, storm surge tracks and magnitudes, oceanic tides, and other factors that affect turbulent mixing can also potentially impact tidal properties within estuaries.

such as wind circulation and wind waves; and (*c*) changes to boundary forcing, including coastal tides and river inflow. As modeled (Godin 1993; Arbic et al. 2009; Müller 2011; Müller et al. 2011; Pickering et al. 2012, 2017; Schindelegger et al. 2018) and reviewed (Hill 2016, Haigh et al. 2019), sea-level rise and other changes in geophysical properties (e.g., stratification) affect oceanic and continental shelf tides, particularly at millennial and longer timescales. Mechanisms of shorter-term tidal fluctuations with sea level were also discussed by Devlin et al. (2014, 2017). This review focuses on tidal evolution in estuaries, embayments, and rivers, based on the observation that the largest changes in tide properties typically occur landward from the coast. Since the global population in low-elevation coastal zones is projected to surpass 1 billion by the year 2060 (Neumann et al. 2015), characterization and understanding of the contribution of altered tides to inundation hazard have broad implications for future coastal resilience.

Both data and numerical models suggest that some estuaries are extremely prone to tidal evolution, while others are relatively impervious. Many regions exhibit a moderate change in tidal range

(<10%) after depth, width, and length changes (e.g., Chant et al. 2018, Talke et al. 2018), while at other locations the tidal range more than doubles (DiLorenzo et al. 1993, Winterwerp et al. 2013, Familkhalili & Talke 2016, Ralston et al. 2019). Why are some locations much more sensitive to altered geometry than others? What are the implications for communities adapting to spatially varying rates of sea-level rise and vertical land motion? How will tide dynamics and nonlinear feedbacks with morphology influence future flooding? What are possible ecological impacts? To address these questions and determine future research needs, we describe empirical data, analyze selected theoretical results, review model results, and discuss implications for the future.

EMPIRICAL EVIDENCE OF CHANGING TIDES

Tidal properties and constituent amplitudes are changing worldwide, at rates much higher than can be explained by changes in astronomical forcing (Woodworth 2010). Multiple empirical studies attest to changes in tide properties over decadal and century timescales. Doodson (1924) commented on nonastronomical changes at Saint John, Canada, while Marmer (1935) and Schureman (1934) discussed how dredging had affected tide properties in the Hudson River estuary (see also Ralston et al. 2019). Cartwright (1972) estimated that the M_2 amplitude in Brest, France, has increased by approximately 1% per century since the early 1700s, and Amin (1983) evaluated changes on the Thames estuary. More recently, Flick et al. (2003) demonstrated that tidal range had changed all over the United States, while Ray (2006) showed that Gulf of Maine tidal amplitudes were increasing (see also Godin 1995, Greenberg et al. 2012, Ray & Talke 2019). Large decadal trends have been observed along the Dutch and German North Sea coasts (Hollebrandse 2005, Jensen & Mudersbach 2007) and in Southeast Asia (e.g., Cai et al. 2012a, Song et al. 2013, Feng et al. 2015). Jay (2009) showed that M_2 and K_1 amplitudes are changing over much of the eastern Pacific, with most of the largest trends occurring in estuaries and tidal rivers such as the Columbia (Jay et al. 2011). Woodworth (2010) and Mawdsley et al. (2015) extended these regional analyses to show that trends occur on decadal and century timescales all over the world. While timing problems and other tide gauge issues sometimes produce spurious trends (Zaron & Jay 2014), the global pattern of changes clearly demands dynamical explanations.

Figure 2 shows variations and trends in tidal range along the US East Coast from as early as 1825, using data discussed by Talke & Jay (2013, 2017). The 18.61-year nodal variability is prominent in most records. After the nodal cycle is accounted for (see Woodworth 2010), many locations show nonastronomical trends that exceed natural variability. Since the mid-nineteenth century, the mean tidal range decreased by 8–9% in Norfolk, Virginia; Washington, DC; and Providence, Rhode Island (decreases of approximately 0.06, 0.08, and 0.12 m, respectively). The tidal range in Boston decreased by 5.5% (nearly 0.2 m) between 1825 and 1910 (Talke et al. 2018). The tidal range in Sandy Hook, New Jersey, decreased at a rate of 3.4% per century from 1844 to 1918 but increased by 3.2% per century after 1932 (Talke et al. 2014) (**Figure 2*a***). In some locations, the tidal range has more than doubled (**Figure 2*b***). The tidal range in Wilmington, North Carolina, has increased by approximately 0.57 m since 1887, while the tidal range in the Longbranch neighborhood of Jacksonville, Florida, increased from 0.33 to 0.77 m. These nonastronomical changes are ubiquitous; only 2 out of approximately 20 US East Coast stations with records longer than 80 years have a trend in tidal range of less than ±1% per century (Fort Pulaski, Georgia, and Fernandina Beach, Florida).

However, except within semienclosed oceanic basins such as the Gulf of Maine (Ray 2006), the North Sea (Hollebrandse 2005, Jensen & Mudersbach 2007, Pickering et al. 2012, Idier et al. 2017), and basins in Southeast Asia (e.g., Pickering et al. 2017), there are few coherent (correlated) trends in tide properties on a regional or global scale that exceed natural variability. The decrease

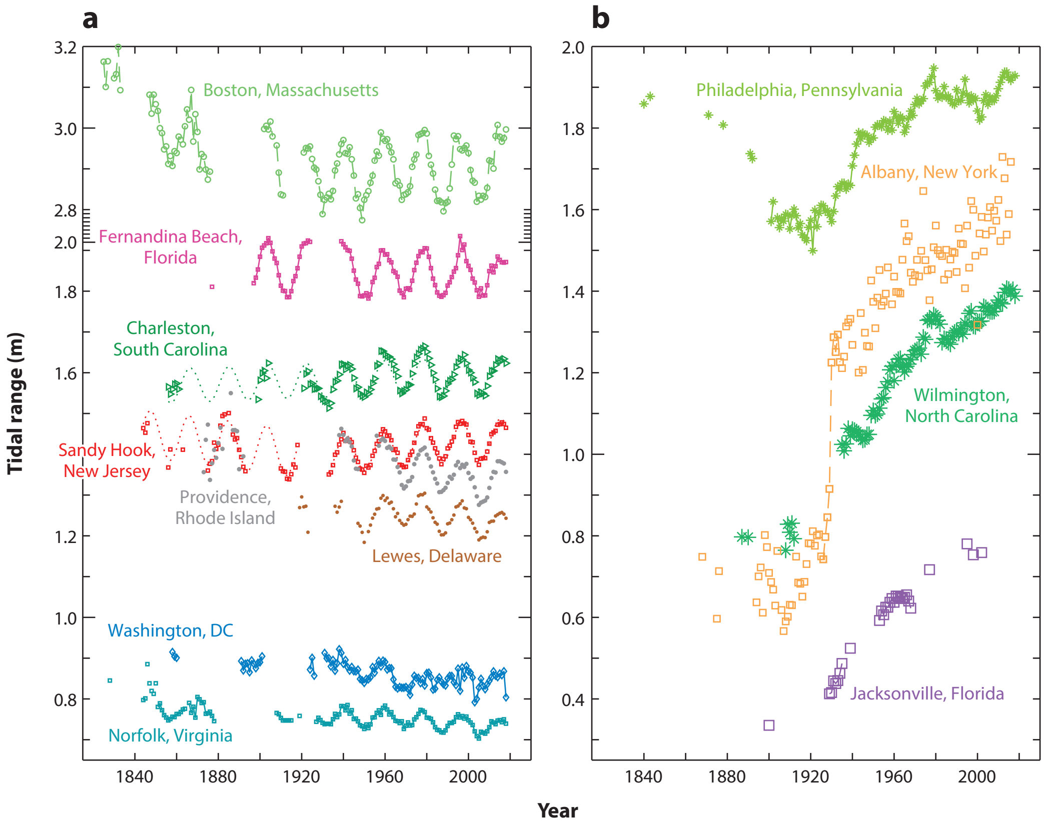

Figure 2

Examples of (*a*) minor or moderate changes and (*b*) major changes in tidal range for selected locations along the US East Coast with long records. The plots are a combination of NOAA data and archival records described by Talke et al. (2014, 2018), Familkhalili & Talke (2016), Talke & Jay (2017), and Ralston et al. (2019). The dashed lines for Sandy Hook and Charleston show how a best-fit regression line that includes a trend and nodal cycle is fit to the data, following the method of Woodworth (2010).

in the S_2 constituent in the northwestern Atlantic is an exception (Ray 2009). Furthermore, Devlin et al. (2014, 2017) found few regional correlations between tide property anomalies and annual sea-level anomalies, though some locations, such as the Solomon Islands, often exhibited a strong response. These considerations support the thesis that nonastronomical trends in tidal properties are driven primarily by local alterations in estuarine properties such as depth, width, length, and bed roughness (see **Figure 1**). Nonetheless, because harbor modification and climate change effects on sea level and river flow are ubiquitous worldwide, changing tides have a global footprint.

Tidal evolution tends to increase as one moves away from the ocean, and the largest changes and variability are often observed in fresh water, in tidal rivers (Winterwerp et al. 2013). The magnitude of changes often exceeds both twentieth-century sea-level rise of 0.14–0.19 m (Church & White 2011, Hay et al. 2015) and the approximately ±3% natural variability in tidal range over an 18.61-year nodal cycle. For example, tidal range in the upstream reaches of the Hudson River more than doubled over a 150-year period (Ralston et al. 2019), with tidal range in Albany increasing from 0.67 to 1.57 m (**Figure 2**). By contrast, the Hudson River estuary (New York Harbor) has shown a more modest twentieth-century evolution, with location-dependent tidal trends of 5–10% (Talke et al. 2014, Chant et al. 2018, Ralston et al. 2019). Similarly, the tidal range in Trenton, New Jersey, on the Delaware River has nearly doubled since the early 1900s, from 1.3 to 2.45 m, and the Philadelphia tidal range has increased by 0.3 m, despite a decreasing trend at the coast of nearly 2% per century at Lewes, Delaware (DiLorenzo et al. 1993) (**Figure 2**). For yet-unexplained reasons, archival records also suggest that the tidal range in Philadelphia dropped by approximately 0.3 m between 1840 and 1900 (**Figure 2**).

Many instances of evolving tidal properties are tied to navigation improvements. Channel deepening has amplified tidal range throughout the Scheldt estuary, with an approximately 1-m increase in tidal range near the upstream boundary since 1900 (Winterwerp et al. 2013). The tidal ranges in the Ems and Loire estuaries have increased by a factor of five at the head of tides since about 1900 (Talke & Jay 2013, Winterwerp et al. 2013), and the tidal range in Bremen, Germany, on the Weser estuary, increased by more than a factor of 10 (from ∼0.25 m to ∼4.25 m between 1885 and 1985; Winterwerp & Wang 2013). Other estuaries and tidal rivers in which dredging and environmental change have altered tide properties and increased amplitudes include the Gironde estuary (Jalon-Rojas et al. 2018), the Cape Fear estuary (Familkhalili & Talke 2016), the St. Johns River estuary (S.A. Talke, R. Familkhalili & D.A. Jay, manuscript in preparation), the Chesapeake Bay estuary (Ross et al. 2017), the Pearl River estuary (Zhang et al. 2010), the Delaware River (DiLorenzo et al. 1993, Ross et al. 2017), the Rotterdam waterway (van Rijn et al. 2018), the Modaomen waterway (Cai et al. 2012b), and the Columbia River (Jay 2009, Jay et al. 2011, Helaire et al. 2019).

As discussed below, large changes within tidal rivers occur due to the cumulative effect of changes further seaward, often in conjunction with a reflective boundary. Tides are also inherently more variable upstream due to the influence of river flow on friction and energy dissipation, and therefore on tide statistics (e.g., Godin 1991, 1999; Kukulka & Jay 2003a; Cai et al. 2012a, 2014; Matte et al. 2013, 2014; Moftakhari et al. 2013, 2016; Guo et al. 2015; Losada et al. 2017). At high river discharge, tides may even disappear within upstream reaches. Alterations in river flow patterns and magnitudes over the past century can therefore influence trends in tidal amplification (e.g., Jay et al. 2011, Ralston et al. 2019). A larger tide also increases the friction felt by river flow and increases the mean river slope (Kukulka & Jay 2003a,b). Hence, within a tidal river, the lowest water levels occur on neap rather than spring tides (due to both larger damping of spring tides and the resulting larger river slope), and the point where the lowest low waters begin to be on neap tides is the seaward boundary of the tidal river (Jay et al. 2015, Hoitink & Jay 2016). Both factors—increased long-wave magnitudes and altered river slope—must be considered when assessing changes to extreme water levels within a tidal river (Helaire et al. 2019, Ralston et al. 2019).

At many locations, tide properties vary approximately linearly through time, after adjusting for the 18.61-year nodal variation (e.g., **Figure 2**). Thus, compilations of tide change typically assess linear trends (e.g., Jay 2009, Woodworth 2010). This assumption appears to be justified for relatively small perturbations in sea level and water depth (Idier et al. 2017). However, long-term patterns are sometimes nonlinear (e.g., **Figure 2*b***), likely because environmental changes can be of large magnitude, episodic (dredging or land reclamation), or driven at nonlinear rates (sea-level rise). In fact, multiple studies show that trends can change sign over long, decadal-to-century timescales (e.g., Talke et al. 2014, 2018). In Sacramento, California, tides disappeared in the late 1800s due to widespread sedimentation caused by hydraulic mining (Gilbert 1917) but have since rebounded due to clearing and dredging of the channel. Similarly, the tidal range in New York City and Sandy Hook, New Jersey, decreased between the 1840s and the 1920s (Talke et al. 2014) but trended upward thereafter, in part because of local dredging and land reclamation (Marmer 1935, Ralston et al. 2019) (**Figure 2**).

REASONS FOR TIDE CHANGES

We next review how changes to friction (energy dissipation) and reflection (resonance) help explain how bathymetric alterations and sea-level rise can cause diverse tidal responses in shallow systems. Energy dissipation is influenced by the rate at which energy is extracted from an environmental flow and converted into turbulent motions (Tennekes & Lumley 1990). Therefore, any environmental change that alters the production of turbulent kinetic energy can potentially affect the energy extracted from tide motions, particularly if the change is large and/or system-wide. Processes that inhibit turbulence production and dissipation and affect tides include the formation of fluid mud (Gallo & Vinzon 2005, Chernetsky et al. 2010, Winterwerp et al. 2013, Dijkstra et al. 2019) and vertical density stratification (e.g., Garrett et al. 1978, Müller 2012, Katavouta et al. 2016, Devlin et al. 2018). Similarly, biotic features such as oyster shells and submerged aquatic plants produce frictional drag and dissipation (e.g., Nepf 1999), such that their removal can produce system-scale effects (e.g., Orton et al. 2015). Removing obstacles and straightening a channel also reduces the effective drag. By contrast, engineered structures such as bridge piers, pile dikes, wharves, and rip-rap groins tend to increase mixing and dissipation (see, e.g., Talke et al. 2010); similarly, flow over ripples and dunes produces coherent turbulent structures that extract energy from the mean flow (Best 2005, Talke et al. 2013). Alterations to such natural roughness features caused by dredging, sand mining, trawling, or changes to sediment supply (e.g., Kenchington et al. 2007, Barnard et al. 2011, Templeton & Jay 2013) can also produce system-scale effects on tides (e.g., Jay et al. 2011, Rodríguez-Padilla & Ortiz 2017). Nonlinear interactions between tidal currents and wind waves also affect drag on tidal flats and other shallow subtidal regions (e.g., Talke & Stacey 2003) in ways that depend on sea-level rise (Arns et al. 2017). The net effect of these many environmental changes on tides can sometimes be estimated inferentially, through changes to the effective drag coefficient used to calibrate and validate numerical models (e.g., Orton et al. 2015, Helaire et al. 2019).

The depth of an estuary also affects frictional damping (e.g., Friedrichs & Aubrey 1994) and impacts energy dissipation, which scales as the cube of velocity over depth (U^3/h) (Simpson & Hunter 1974). Mathematically, the effects of depth changes are often modeled through a friction coefficient that depends on $1/h$, where h is the depth (Jay 1991, Friedrichs & Aubrey 1994) (see below). Qualitatively, depth matters because surface flows "feel" the slowing effect of the bed much less in a deep channel than they do in a shallow channel. Effectively, turbulent motions that reduce fluid velocity are not transmitted as effectively to the surface as water depth increases (Talke et al. 2013). The observation that turbulent motions are less likely to break the surface in deep water is enshrined in the aphorism "still waters run deep."

To gain insight into how tides propagate and evolve in estuaries, and are affected by friction, many approximate or semianalytical solutions to the shallow-water equations (defined in the **Supplemental Appendix**) have been developed using different scaling assumptions, bathymetric representations, and boundary conditions (LeBlond 1978, Prandle & Rahman 1980, Jay 1991, Friedrichs & Aubrey 1994, Lanzoni & Seminara 1998, Godin 1999, Li & Valle-Levinson 1999, Prandle 2003, Savenije & Veling 2005, Toffolon & Savenije 2011, van Rijn 2011, Winterwerp & Wang 2013). Various channel cross sections have been used (with or without tidal flats); similarly, different representations of width convergence have been used (e.g., constant width and linear, geometric, and exponential variation) to simulate along-channel dynamics. At the open boundary, tidal elevations are typically prescribed, though sometimes a system coupled to a larger ocean basin is used (e.g., Arbic et al. 2009). At the landward boundary, tidal amplitudes are assumed to decrease toward zero or a reflective condition is applied. While most analytical models are confined to a single tide constituent (typically M_2) or a combination of M_2 and M_4 (the first overtide),

Supplemental Material >

multiconstituent models are possible and provide additional dynamical insight (e.g., Giese & Jay 1989, Buschman et al. 2009). More complex models that include the Coriolis force, bathymetric variation, density gradients, and turbulence closure require numerical solutions (e.g., Ensing et al. 2015, Dijkstra et al. 2017). For reference, an open source tide solver is embedded in the iFlows model (Dijkstra et al. 2017), and analytical solutions have been tabulated by van Rijn (2011) and Winterwerp & Wang (2013).

Supplemental Material >

In their simplest form, the shallow-water equations used to model tides (see the **Supplemental Appendix**) can be reduced to a differential equation (the wave equation) that is forced by cyclic (sinusoidal) motions at the boundary. The solution is analogous to a driven harmonic oscillation with damping (e.g., Godin 1993, Arbic et al. 2009, Arbic & Garrett 2010). Examples in other fields include a spring-damper system or a swing (e.g., Case & Swanson 1990). When children learn to pump at or near the natural frequency of a swing, they can attain large amplitudes; until they do, amplitudes remain small (e.g., Case & Swanson 1990). Similarly, when gravitational forcing occurs near the natural resonance frequency of a channel-like basin, large-amplitude tides occur (e.g., at the Bay of Fundy; Garrett 1972). Continuing the analogy, frictional forces tend to reduce or damp out oscillations on a swing, when forcing is diminished or removed. Similarly, an increase in tidal energy dissipation and damping tends to diminish tidal amplitudes. However, even a simple damped harmonic oscillator has nonintuitive properties, particularly with regard to sea-level rise and depth changes in an embayment. For this reason, we systematically consider the simplest case first and move to more complex examples later.

Example 1: Tides in Channels of Constant Width and Depth

Globally, many semienclosed basins exhibit amplified tides due to the constructive interference of an incoming and reflected tide wave, with modifications due to convergent geometry. Examples of near resonance at the semidiurnal frequency include Bristol Bay and Cook Inlet in Alaska (Fong & Heaps 1978, Danielson et al. 2011), Long Island Sound (Wong 1990, Kemp et al. 2017), the Gulf of Maine (Marmer 1922, Duff 1970, Garrett 1972, Godin 1993), the Chilean Inland Sea (Aiken 2008), and the Gulf of California (Godin 1993). For diurnal tides (once daily), examples of resonant systems include the Sea of Okhotsk, the Sahul Shelf, and the Gulf of Tonkin (Skiba et al. 2013). Some embayments, such as the Gulf of Carpenteria (Webb 2012) and the Adriatic Sea (e.g., Cushman-Roisin & Naimie 2002, Terra 2005), are resonant in both the diurnal and semidiurnal frequency bands. Other systems, such as Hecate Strait on the west coast of Canada, have resonant periods that are near the quarter-diurnal (four times a day) period of typical shallow water overtides (Foreman et al. 1993). Hence, exploring the dynamics of resonant systems is a good place to begin an exploration of tidal dynamics and changes therein.

In the absence of friction, a theoretically infinite amplitude resonance can be shown to occur (see the **Supplemental Appendix**) when a constant-width channel of constant depth h has a length L that equals

$$L = \frac{(2n-1)T\sqrt{gh}}{4}, \tag{1.}$$

where $n = 1, 2, 3\ldots$; T is the period of an individual tide constituent; and g is the gravitational acceleration. The quantity $\lambda_0 = T\sqrt{gh}$ is the frictionless tidal wavelength, where wavelength is defined as the distance between crests. The first mode, with $n = 1$, occurs at the length scale $l_o = \lambda_0/4$ and is known as quarter-wave resonance. For the M_2 tidal constituent, which has a period of 12.42 h, the length scales l_o for a 10-m- and 50-m-deep channel are approximately 110 km and 250 km, respectively. Because most estuaries and embayments are short relative to λ_0, amplification near the quarter-wave resonance frequency is the most likely mode to be observed. (Three-quarter-wave resonance is possible but rare; see Webb 2012.) The depth dependence in Equation 1 shows that sea-level rise or channel deepening can cause a system to move closer to or farther from quarter-wave resonance.

A more realistic result is achieved when damping is included in an analytical tide model (Dronkers 1964). Amplification due to constructive interference then becomes broadband and bounded—in other words, amplification is observed for a spread of frequencies around a finite peak amplitude. Many natural and engineered systems exhibit similar behavior, because the underlying differential equations are similar (see, e.g., Blanchard 1941); hence, Miles (1971) explicitly compared harbor resonance to an electrical circuit. A solution for tidal amplification in a constant-width channel in which friction has been linearized was described by Dronkers (1964). The amplification A_* at the end of a resonant channel of constant depth is

$$A_* = \sqrt{2}\left[\cosh\left(\frac{2\omega L}{\sqrt{gh}}\sigma\right) + \cos\left(\frac{2\omega L}{\sqrt{gh}}\beta\right)\right]^{-1/2}, \qquad \text{2a.}$$

where

$$\sigma = \sqrt{-\frac{1}{2} + \frac{1}{2}\sqrt{1 + \left(\frac{r}{\omega}\right)^2}}, \qquad \text{2b.}$$

$$\beta = \sqrt{\frac{1}{2} + \frac{1}{2}\sqrt{1 + \left(\frac{r}{\omega}\right)^2}}, \qquad \text{2c.}$$

L is the length of the channel, $\omega = 2\pi/T$ is the angular frequency, and r is the linearized friction coefficient, often approximated as

$$r = \frac{3\pi}{8}\frac{C_d U}{h}, \qquad \text{2d.}$$

where C_d is the drag coefficient, U is the velocity, and h is the depth. When $r/\omega = 0$, the inviscid (frictionless) solution is recovered (see the **Supplemental Appendix**). More physically realistic geometries that include depth variations, width convergence, and forcing that includes Coriolis effects are considered elsewhere (e.g., Prandle 1991). Moreover, as Godin (1993) showed, the tides in a sub-basin modify the ocean tides and vice versa (see also Arbic et al. 2009, Arbic & Garrett 2010), such that a coupled spring-damper system is more appropriate. These studies show that some commonly cited properties of resonant systems (such as the presence of nodes with zero amplitude) are usually not observed in real systems like the Bay of Fundy.

Supplemental Material >

However, the simplicity of the model geometry used in Equations 2a–d provides many interesting insights about resonant systems in the presence of friction and how they might be altered by changing environmental conditions and sea-level rise, particularly when the Coriolis force and width/depth variations only modify, rather than drive, the system response. **Figure 3** depicts how amplification at the closed channel boundary varies as a function of normalized channel length (L/λ_0) and friction (r/ω) and shows the following to first order:

- Increased damping reduces maximum amplification. As frictional effects become larger (r/ω increases), the amplification at the head of tides decreases. However, the spread of frequencies (wave periods) over which at least some amplification is found increases. Effectively, resonance transitions from a sharp discontinuity in a frictionless system to a broadband phenomenon.

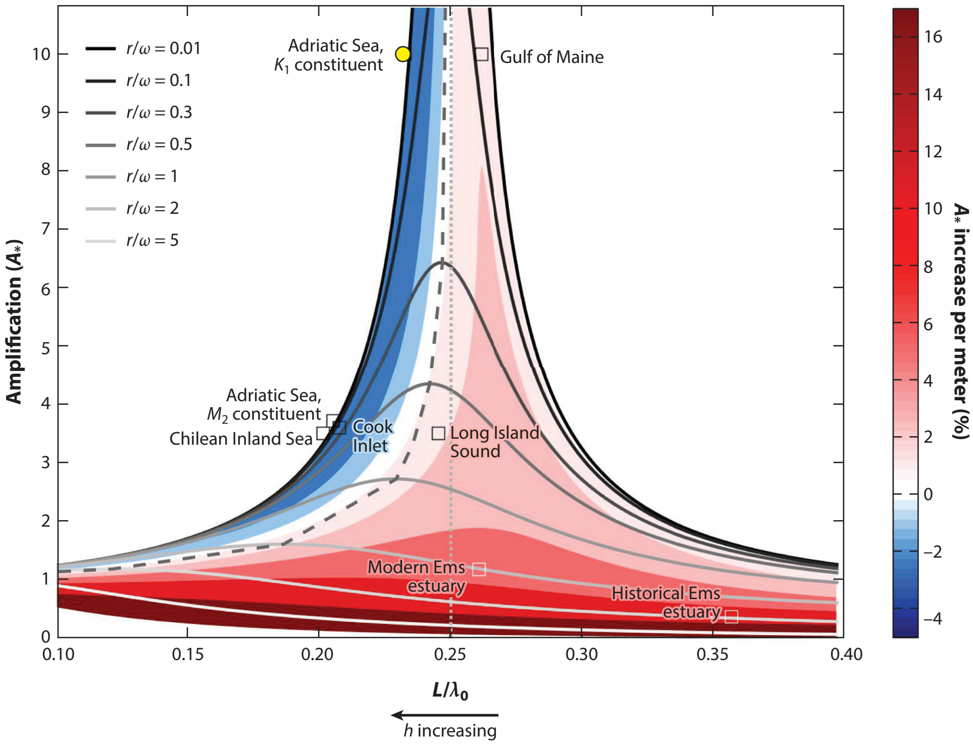

Figure 3

Amplification of tide magnitude (A_*) at the head of a channel relative to the amplitude at the open boundary (Equation 2). As the length L of a channel approaches the inviscid quarter wavelength $\lambda_0/4 = 0.25T\sqrt{gh}$, large amplification occurs. Contour lines of constant r/ω show how amplification is modified by frictional effects. The approximate locations within this parameter space of either the M_2 or K_1 constituent in real systems (idealized as channels) are shown as squares and circles. Colors indicate the percentage change in amplitude at the head of tides that occurs for a 1-m increase in depth (sea level)—i.e., showing $A_*(h)/A_*(h+1)$. Increasing depth moves a system left along the x axis (as shown) and alters amplification. Amplification and the L/λ_0 ratio (or, equivalently, basin resonance period over tide wave period) are based on references in the main text. The parameter space for K_1 and M_2 in the Adriatic Sea is based on observations of oscillation modes of approximately 22 and 11 h, respectively.

- The wave period at which maximum amplification occurs becomes larger as friction (r/ω) increases, because friction slows the propagation speed of a wave. This is shown by the dashed line in **Figure 3**.
- Sea-level rise and other depth changes alter both the resonant frequency (which depends on $\sqrt{h}$) and frictional effects (which vary with $1/h$). As depth increases, the solution moves toward a smaller r/ω contour (i.e., up the y axis in **Figure 3**) and moves to a smaller L/λ_0 ratio (i.e., moves left on the x axis in **Figure 3**).
- Changes in the drag coefficient alter only the friction r/ω and are independent of the x axis in **Figure 3**—i.e., they produce only a change in amplification. Reduced frictional drag increases amplification.
- Changes in estuary length alter amplification. To a first approximation, the friction r/ω is independent of the estuary length L (a slight dependence enters through any velocity changes). Hence, changing the length of a system will produce a response that follows the r/ω contour. For systems with a length below the resonant frequency, increasing length

(moving to the right along an r/ω contour) causes increased amplification; for systems such as the Bay of Fundy, which are above this threshold (at M_2 frequency), a decrease in length would produce amplification (**Figure 3**).

- Systems near (but not at) resonance are most sensitive to length changes. The largest sensitivity to a length alteration occurs when the steepness (slope) of the r/ω contour is maximal. Hence, the model predicts that the largest sensitivity occurs at $L/\lambda_0 \sim 0.2$–0.24 and $L/\lambda_0 \sim 0.26$–0.3 (**Figure 3**). Because the Gulf of Maine resonance period is 12.5–13.3 h (see Garrett 1972, Greenberg et al. 2012), it is within the region of large sensitivity to length changes for the M_2 tidal frequency, as shown in **Figure 3**. Therefore, decreases in length caused by road construction and morphological changes in the 1960s and 1970s (Daborn & Dadswell 1988) may have increased M_2 amplification. Conversely, numerical models suggest that flooding induced by sea-level rise in the Gulf of Maine could increase length and decrease the amount of amplification (Pelling & Green 2013). Similarly, Terra (2005) found that M_2 resonance in the Adriatic Sea decreased over geologic timescales, due to increasing length.
- Depth changes can either amplify or decrease tidal range. Increased depth causes the system to jump toward a smaller r/ω contour and also decreases L/λ_0 in a way that can lead to either amplification or diminution.

To emphasize the last point and explore the effect of sea-level rise in an idealized embayment, we overlay the contours in **Figure 3** with the percentage change in amplification at the head of tides that occurs due to a 1-m increase in the depth h (for the calculation details, see the **Supplemental Appendix**). Interestingly, the percentage change in amplification is strongest in systems that are highly damped ($r/\omega > 2$), i.e., systems that are shallow or have high drag. At the semidiurnal tidal frequency, a system that would most closely approximate the highly damped system is an approximately 10-m-deep channel with a barrier between 70 and 130 km from the coastal ocean. While the typical coastal plain estuary is funnel shaped (i.e., not constant in width or depth), many do have a length scale within this range (e.g., Lanzoni & Seminara 1998). Such estuaries (e.g., the Thames and Severn estuaries; Liang et al. 2014) are often highly amplified at the head of tides. We discuss such amplification in more detail below; for now, we note that tidal range in the Ems estuary greatly increased after the construction of a weir approximately 100 km from the coast around 1901, consistent with wave reflection and the formation of resonance (Talke & Jay 2013) (**Figure 4**). Amplification at the weir continued to increase as depth was increased from approximately 4 m to 7 m (today), and the historical trajectory can be approximated by a combination of this depth change and a decrease in the friction parameter $r/\omega = 2$ to $r/\omega = 1$ (i.e., the system moves from the historical situation to the modern, as shown in **Figure 3**). As discussed below, including the effects of width convergence modifies this solution (see also Ensing et al. 2015 and the **Supplemental Appendix**). Nonetheless, the simple model (Equation 2) highlights the importance that changing depth has on effective friction and wave speed and therefore on wave reflection and resonance. Equation 2 also qualitatively explains many observed changes to tides.

Supplemental Material >

Figures 3 and **4** show, therefore, how shallow estuarine systems—if subject to channel deepening, length changes, and/or sea-level rise—can produce amplification in systems that previously appeared damped. An interesting historical case is the Thames estuary, in which tidal range increased from approximately 2 m in Roman times to approximately 8 m during Victorian times (Reidy 2008). Indeed, historical data and qualitative accounts suggest that channel modifications and infrastructure development starting in the second half of the 1700s increased tide magnitudes and currents (e.g., Amin 1983, Reidy 2008); earlier, land reclamation confined flow, and the construction of London Bridge in the late twelfth century approximately 100 km from the coast caused wave reflection, much as building a weir 100 km from the coast altered tide dynamics in

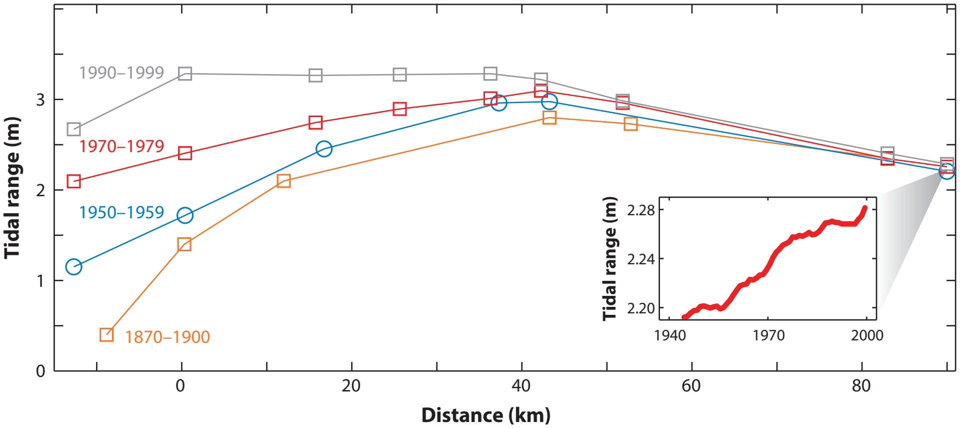

Figure 4

Tidal range in the Ems estuary, Germany, as a function of time and location. The tidal range at the boundary with the North Sea has increased slightly (*inset*; Jensen & Mudersbach 2007). A more than fivefold increase in tidal range occurred near the head of tides after construction of a tidal weir in 1901 at river kilometer −13 and progressive deepening of the shipping channel through the mid-1990s (Chernetsky et al. 2010, Talke & Jay 2013, Winterwerp et al. 2013, de Jonge et al. 2014). The x axis is based on the local coordinate system of river kilometers. Figure adapted from Talke & Jay (2013) with permission from the Coastal Education and Research Foundation, Inc.

the Ems estuary (**Figure 4**). Still, showing more definitely that London Bridge was falling down due to tidal reflection and amplification would require a joint exercise in historical analysis, data archaeology, and estuarine physics.

Deeper embayments with large amplification, such as the Gulf of Maine, are less sensitive to 1 m of sea-level rise than most estuaries and tidal rivers because the fractional change in both resonant frequency and frictional effects is buffered by large depth (**Figure 3**). The estimated sensitivity in Gulf of Maine tides is approximately 2%, i.e., 2 cm per meter of sea-level rise (**Figure 3**), similar to the 2.4–4% sensitivity modeled by Schindelegger et al. (2018). Tides in Long Island Sound are amplifying at a slightly larger rate (∼10% per meter) due to sea-level rise (Kemp et al. 2017) (**Supplemental Figure 1**); the simple channel model in **Figure 3** underestimates the change, likely because width convergence is not considered (see also **Supplemental Figure 2**).

Supplemental Material >

In other resonant systems, such as the Chilean Inland Sea or Cook Inlet, a positive rise in sea level produces a negative excursion in M_2 amplitude (Devlin et al. 2017). Effectively, an increase in depth moves the resonance length scale away from the system length. Cook Inlet provides a fascinating example of how vertical land motion can influence amplification. As in other regions of Alaska, sea level is currently dropping. Because tidal amplitude is anticorrelated with depth (blue shading in **Figure 3**), the M_2 tide (and tidal range) is currently increasing (see also **Supplemental Figure 1**). The opposite effect occurred in response to a magnitude-9.2 earthquake in March 1964, which lowered the seabed and increased relative sea level on the order of 1 m. In response, fragmentary measurements suggest that the M_2 amplitude dropped by approximately 0.2 m between 1963 and 1964 (see **Supplemental Figure 1**).

Convergent, Frictional Estuaries

The Dronkers (1964) analysis (Equations 2a–d) is a useful entry point but is incomplete because it neglects the importance of convergence of cross-sectional area, which has a dramatic effect on wave speed and, therefore, amplification. For a constant-depth estuary with an exponential convergence in width [i.e., $b(x) = b_o \exp(-x/L_e)$], Jay (1991) found that the tidal amplitude can be expressed as

Critical convergence: the condition when acceleration and convergence effects cancel out; at larger convergence (smaller L_e), wave speed increases to values above $\sqrt{gh}$

$$\eta(x,t) = \exp\left(\frac{x}{2L_e}\right) \cdot Re\left[\left(\underbrace{A_o \exp^{iqx}}_{\text{reflected wave}} + \underbrace{B_o \exp^{-iqx}}_{\text{incident wave}}\right)\exp(i\omega t)\right], \tag{3a}$$

where

$$q = \frac{\omega}{\sqrt{gh}}\left(\underbrace{1}_{\text{acceleration}} - \underbrace{\Delta^2}_{\text{convergence}} - \underbrace{\frac{ir}{\omega}}_{\text{friction}}\right)^{1/2} = k + ip, \tag{3b}$$

$$\Delta = \frac{1}{2}\sqrt{gh}/L_e\omega. \tag{3c}$$

Here, Δ is the convergence parameter and L_e is the e-folding scale of width convergence [i.e., the length over which channel width has decayed to $\exp(-1) = 36.8\%$ of the width at the mouth, b_o]. The parameter $k = Re[q]$ is the conventional wavenumber, and $p = Im[q] < 0$ is the damping modulus; it is negative so that the incoming wave damps in the positive x direction ($x = 0$ at the estuary mouth). The constants A_o and B_o depend on the amplitude at the ocean boundary and on whether the tide reflects at the upstream boundary or damps out. When the convergence length scale L_e is infinite and the frictional effects r/ω are small, an inviscid, constant-width solution is found, with a wave speed $c = \omega/k = \sqrt{gH}$. As can be seen in Equation 3b, both the friction and convergence terms modify the wave propagation speed. Friction slows the wave, while convergence increases c.

From this basic equation for a frictional, convergent estuary, several special cases emerge (Jay 1991, Lanzoni & Seminara 1998, Savenije et al. 2008). In most shallow estuaries (<10-m depth), friction dominates over inertial (acceleration) effects—i.e., $r/\omega > 1$ (e.g., LeBlond 1978, Friedrichs & Aubrey 1994, Lanzoni & Seminara 1998, Prandle 2003)—and the estuary is either strongly or moderately dissipative (Lanzoni & Seminara 1998). Systems with a depth much greater than 10 m are usually weakly dissipative.

The effects of width variations are encapsulated in the convergence term in Equations 3a–c. When the convergence term $gh/4L_e{}^2\omega^2 < 1$ in Equation 3b or, equivalently, when the convergence length scale $L_e > \sqrt{gh}/2\omega$, the estuary is weakly convergent. For example, $gh/4L_e{}^2\omega^2 \approx 0.25$ for a semidiurnal tide wave in a 5-m-deep estuary with a width convergence of 50 km (which approximates the St. Johns River in Florida around 1900). Under such conditions, convergence only slightly modifies the solution found for a constant channel width (see the **Supplemental Appendix**). As an estuary deepens (e.g., due to sea-level rise, dredging, or loss of wetlands), a weakly convergent system can shift toward critical convergence. For a constant-depth system, this occurs when $L_e = \sqrt{gh}/2\omega$ or, equivalently, when $L_e = l_o/\pi$, where l_o is the inviscid quarter-wave resonance length scale (Equation 1). When depth varies along channel or intertidal flats are present, the solution is modified (Jay 1991, Winterwerp & Wang 2013). For an M_2 tidal wave, critical convergence occurs for $L_e = 24$ km and 35 km for 5- and 10-m-deep channels, respectively, but bathymetric variability and river flow can alter the critical convergence (e.g., Ensing et al. 2015). In the critical case, the strength of friction determines the properties of the solution, and the phase difference between tidal velocity and water level is 45° (i.e., peak flood occurs approximately 1.5 h before high water).

Supplemental Material >

Example 2: Long, Weakly Convergent Channels

In shallow, frictional river estuaries, the tide often decays to zero before reaching a boundary. If the wave amplitude $\eta \to 0$ as $x \to \infty$, then $A_o = 0$ in Equation 3a and only an incident wave is found. In weakly convergent, strongly frictional estuaries, scaling suggests that both the acceleration term and the convergence term in the definition for q (Equation 3b) are unimportant relative to the frictional term (LeBlond 1978, Jay 1991, Winterwerp & Wang 2013). Taking the absolute value of the solution (Equations 3a–c) to remove time dependence, one finds that tide magnitudes decay exponentially as one moves upstream (S.A. Talke, R. Familkhalili & D.A. Jay, manuscript in preparation; see also Winterwerp & Wang 2013):

$$\eta\,(x) \approx \eta_o \exp(\mu x), \tag{4a}$$

where

$$\mu = p + 1/2L_e, \tag{4b}$$

$$p \approx -\omega(c_d \eta L)^{1/2}/\sqrt{gh^3}. \tag{4c}$$

Here, p is the damping modulus and μ is the damping rate modified by convergence (for a similar result, see van Rijn 2011). In Equation 4c, L is the length scale that controls the tidal prism and is either the length scale over which width convergence occurs (L_e) or the length that tides intrude, whichever is shorter. From Equations 4a–c, one can infer that the e-folding length scale for tides to decay to $\exp(-1) \sim 37\%$ of their boundary value will increase as μ decreases in magnitude. Because p and $1/2L_e$ in Equation 4b have opposite signs, convergence tends to increase the e-folding length scale of tide damping. Intuitively, funneling tends to increase amplitudes.

Equations 4a–c also suggest that increasing the depth of strongly frictional estuaries will decrease damping, as will reductions in the drag coefficient. For example, fluid mud reduced the hydraulic drag in the Ems estuary and contributed to increased tidal amplitudes (Talke et al. 2009b, Chernetsky et al. 2010, Winterwerp et al. 2013, van Maren et al. 2015, Dijkstra et al. 2019) (**Figure 4**). Similarly, Wang et al. (2014) found that episodic high-sediment concentrations affected tides in the Guadalquivir estuary in Spain. Strong salinity stratification within an estuary has a similar effect on tides by reducing the drag coefficient (Giese & Jay 1989, Jay et al. 1990). Thus, the increase in tidal range in San Francisco (Jay 2009) may in part be related to a reduction in drag caused by the removal of large-scale dune features (Rodríguez-Padilla & Ortiz 2017), in addition to a slight change caused by a long-term reduction in river discharge (Moftakhari et al. 2013).

Perhaps not as obviously, the damping in frictional estuaries also depends on its length L (e.g., Du et al. 2018), wave frequency, and amplitude η. Both amplitude and length influence the tidal prism and hence the tidal velocity; similarly, the timescale over which tides enter and exit an estuary influences the current strength (e.g., Friedrichs & Aubrey 1994, Friedrichs 2010). Hence, all else being equal, a diurnal wave is less influenced by friction than a semidiurnal wave. However, the dominant constituent (usually M_2) typically damps a small constituent (e.g., K_1) more than the small constituent (K_1) affects the larger, because the velocity in the linearized friction term (Equation 2d) is the total velocity associated with all the constituents and river inflow (Godin 1986, Jay et al. 2015). Empirical studies attest to the influence of amplitude and frequency; for example, Jay et al. (1990) showed that spring tides are damped more than neap tides, while Díez-Minguito et al. (2012) showed that the amount of reflection (i.e., the amplitude at the head of tides) depends on wave frequency.

From Equations 4a–c, S.A. Talke, R. Familkhalili & D.A. Jay (manuscript in preparation) showed that long-wave amplitudes evolve in a predictable way along the axis of a frictional estuary as depth h or length L is changed. Taking the partial derivative of Equation 4 with respect to h, one can show that the change in tidal amplitude, $\Delta\eta$, varies in the x direction with the proportional change in depth, $\Delta h/h$:

$$\Delta\eta = \left(\frac{-3}{2}\right) p\eta_o x \cdot \exp(\mu x)\frac{\Delta h}{h}. \tag{5}$$

From Equation 5, we infer that the largest $\Delta\eta$ in a nonreflective estuary occurs when the damping magnitude μ is large and the tide decays spatially. In the St. Johns River estuary, tidal range in 1900 decreased from 1.3 to 0.3 m between the coast and Jacksonville, 40 km inland. Since damping was large, channel deepening from 5.5 m to approximately 12 m greatly amplified tidal range (S.A. Talke, R. Familkhalili & D.A. Jay, manuscript in preparation) (**Figure 2**). By contrast, tidal range in New York Harbor is nearly constant (small damping), which may help explain why large-scale deepening and infrastructure projects have changed tidal amplitudes by only 5–10% (Chant et al. 2018, Ralston et al. 2019). The proportional change in depth, $\Delta h/h$, also matters (Equation 5); an example is the Cape Fear estuary, in which a doubling of channel depth has more than doubled tidal amplitudes in Wilmington, North Carolina (Familkhalili & Talke 2016) (**Figure 2**). Finally, Equation 5 suggests that changes in tidal amplitude are spatially variable according to $x \cdot \exp(\mu x)$; this is a parabolic-like function with an amplitude of zero at the estuary boundary and far upstream. Hence, effects of tide changes such as increased flood risk are not evenly distributed. Typical locations for maximum change in tidal range are 60 km (as in the Columbia River estuary) and 20 km (as in the St. Johns River estuary in Florida) (Helaire et al. 2019; S.A. Talke, R. Familkhalili & D.A. Jay, manuscript in preparation).

Example 3: Exponentially Converging Estuary with Reflection

In a convergent estuary with a reflective boundary (e.g., a weir, dam, or natural rock formation), the energy of the incoming wave is funneled into increasingly small cross sections, where it is reflected and travels seaward, toward ever larger cross sections. Because the outgoing reflected wave is diminished by both friction and divergence (increased width), its amplitude tends to damp out relatively quickly (Green 1837, Jay 1991). Hence, constructive interference between the incoming and outgoing waves is typically most prominent at the landward boundary, and the largest tide change over time in a reflective system usually occurs near this point (Chernetsky et al. 2010, Winterwerp et al. 2013, Ensing et al. 2015, Ralston et al. 2019). Hence, in the Ems, tide changes close to the tidal weir (located at river kilometer −13) are much larger than those near the coast (**Figure 4**). The observation that tidal amplification is largest near a reflective boundary differs notably from estuaries without a reflection, since in those systems maximum changes occur much closer to the coast (see example 2 above). Solutions for a system with reflection were tabulated by van Rijn (2011) and Winterwerp & Wang (2013) and involve applying the boundary condition that no flow occurs through the boundary.

We next explore how the maximum amplification (compared with tides at the estuary mouth) changes as a function of the convergence parameter $\Delta = \pi l_o/L_e = \frac{1}{2}\sqrt{gh}/L_e\omega$ (Equation 3c) and the friction parameter r/ω (Equation 3b; **Figure 5*a*,*b***). To find this length scale, we varied the estuary length for each value of Δ and r/ω until the maximum amplification was found; the result is a measure of the potential amplification that an estuary can have for a given convergence and friction, and actual amplification may be less, depending on the length of an individual estuary. For cases in which tides are strongly damped, the maximum tide is found at the ocean boundary, and the ratio is equal to one.

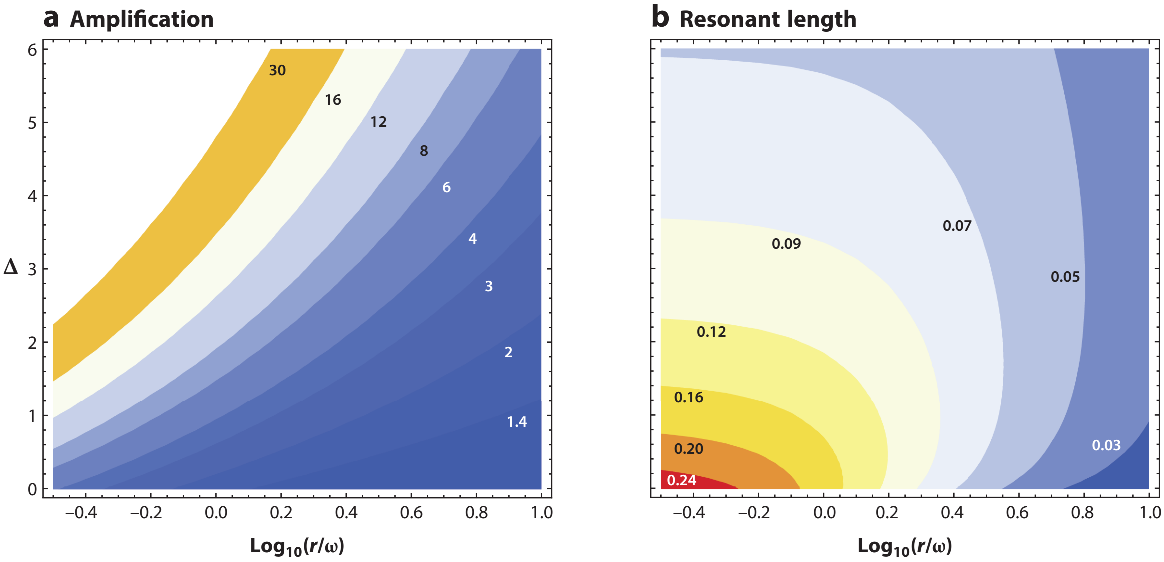

Figure 5

(*a*) The maximum amplification possible under linear theory in a convergent estuary with reflection. Amplification is defined as the ratio of the maximum tidal amplitude within the system to that at the boundary and is shown by the contour labels. As the friction parameter r/ω decreases due to depth increases, amplification increases. Similarly, as the convergence parameter $\Delta = \frac{1}{2}\sqrt{gh}/L_e\omega$ increases, amplification also increases. (*b*) The length of maximum amplification, normalized by the inviscid tidal wavelength $\lambda_0 = T\sqrt{gh}$; this is at the entrance for strong friction but approaches the quarter wavelength ($\lambda_0 = 0.25$) for weak convergence and friction. The contours show different values of L/λ_0.

Figure 5 shows that maximum amplification in reflective systems occurs when frictional effects (r/ω) are small and convergence Δ is large (or, stated differently, the *e*-folding length scale for width, L_e, is small compared with the quarter-wave resonance length scale). Similarly, the combination of strong friction (large r/ω) and weak convergence (small Δ) produces tide waves that decay monotonically from the boundary. Within estuaries, typical values for r/ω (Equation 2d) lie between 1 and 10, while the typical values of Δ (Equation 3c) lie between 0 and 3 (Lanzoni & Seminara 1998, Prandle 2003). The low-friction, high-convergence corner of the parameter space (upper left of **Figure 5*a***) leads to unrealistic amplification, so shading was omitted. The case of $\Delta = 0$ (no convergence) in **Figure 5*a*** corresponds to the dashed line in **Figure 3** that shows how maximum amplification changes with different r/ω contours.

Figure 5*a* suggests two ways in which sea-level rise and dredging can potentially increase amplification. First, sea-level rise (increasing h) increases $\Delta = \sqrt{gh}/L_e\omega$, effectively moving the estuary up the y axis of **Figure 5*a***. At the same time, the friction parameter $r/\omega \sim C_d U/h\omega$ will decrease, moving the solution leftward along the x axis. The Ems estuary (**Figure 4**) is a canonical example of both effects; since around 1900, increased depth from approximately 4 to 7 m has increased the convergence parameter Δ from 0.75 to approximately 1. Moreover, frictional effects decreased r/ω from 7 to 1.7 (Winterwerp et al. 2013), due to both deepening and decreased drag (see also Chernetsky et al. 2010). In physical terms, the convergence effects in Equation 3 have increased and frictional effects have decreased, both of which worked to amplify tides (**Figure 4**). Therefore, the amplification suggested by Equation 2 (**Figure 3**) for a 1-m change in depth will be modified, and usually increased, by convergence effects (see the **Supplemental Appendix**). The largest changes occur for shallow (<10 m) systems rather than deeper (>10 m) systems.

Supplemental Material >

Increasing frictional effects (larger r/ω) also tends to reduce the length of an estuary at which maximum amplification (resonance) occurs (**Figure 5*b***). For a weakly frictional system (left side of **Figure 5*b***), resonance occurs near the quarter-wave length scale, i.e., at a normalized length near 0.25. Strong friction both damps the maximum amplification and causes it to occur at a fraction of the quarter-wave resonance length scale. Increasing the convergence parameter (Δ) also tends to decrease the length of the reflective estuary at which maximum amplification occurs. Other aspects of reflection have been discussed by Díez-Minguito et al. (2012) and Garel & Cai (2018).

The amount of convergence determines how a system will react to depth changes. Ensing et al. (2015) showed that, within the Ems estuary, tidal amplitude increased as convergence Δ is increased until a peak-resonance condition is reached at $\Delta = 2.15$ (their parameter $\mu = 4.3$), after which amplitudes slightly decreased. Similarly, the analytical model results of Cai et al. (2012b) suggested that tides in some estuaries would decrease with sea-level rise, though most would increase. Interestingly, Ensing et al. (2015) found that ~5 m of dredging is needed to attain peak amplitude at the upstream boundary, compared with 2.8 m of sea-level rise. This occurred because sea-level rise also increased water levels on the shoals, while dredging did not. Hence, while historical dredging effects may provide a useful preview of future effects of sea-level rise, subtidal and intertidal regions are also important and differentiate the two processes.

Land Reclamation, Land Inundation, and Other Shallow-Water Effects

Wetland reclamation has occurred for many centuries (e.g., Seasholes 2003) and continues today (Murray et al. 2014). However, sea-level rise may permanently flood regions that were formerly behind dikes or otherwise protected (e.g., Pelling & Green 2013). How susceptible are tides in estuaries to changes in the extent of subtidal, intertidal, and wetland areas?

Numerical models suggest that the aerial extent of floodplains, wetlands, and intertidal flats significantly affects tidal properties (e.g., Pelling et al. 2013a, Holleman & Stacey 2014). For example, including the wetting and drying of extensive tidal flats in a numerical model of Cook Inlet increased the tidal range by approximately 20% (Oey et al. 2007). Similarly, including lagoons in a numerical model of the Adriatic Sea increased M_2 amplitudes (Ferrarin et al. 2017). By contrast, Holleman & Stacey (2014) modeled a decrease in tidal range within the southern San Francisco Bay when overland flooding of diked regions was allowed.

Land reclamation also produces variable results on tides. In China's Xiangshan Bay, reclamation of tidal flats between 1963 and 2010 was modeled to decrease the M_2 amplitude by 6% (0.1 m) but increase the M_4 overtide by 27% (0.09 m) (Li et al. 2018). A 5.5% decrease in tidal range, coupled with an increase in the M_4 overtide and decrease in the M_6 overtide, was observed in Boston Harbor (Talke et al. 2018). Since the M_4 (four times a day) and M_6 (six times a day) overtides are formed by different nonlinear interactions involving the main M_2 constituent (Parker 1991), Talke et al. (2018) inferred that land reclamation in the nineteenth century was the primary cause. Within Jiaozhou Bay, China, the modeled M_2 decreased by approximately 4% and M_4 increased, both of which were a result of large-scale reclamation and altered bathymetry (Gao et al. 2014). In contrast to these examples of M_2 decrease, Song et al. (2013) found that removal of tidal flats resulted in a 0.11-m increase in regionally averaged M_2 amplitudes in the East China Sea.

Both energy and mass-balance considerations influence tidal amplitudes when tidal flats and other shallow bathymetry are present and account for the diverse results described above. Tidal flats and subtidal regions are sinks of energy (e.g., Speer & Aubrey 1985, Song et al. 2013, Holleman & Stacey 2014) and thus influence damping. The presence of tidal flats and subtidal areas also changes the effective depth and convergence of an estuary (e.g., Jay 1991, Ensing et al.

2015), affecting both the frictional damping and reflection shown in **Figures 3** and **5** (see also Holleman & Stacey 2014).

Finally, analytical models suggest that mass-balance considerations may play a significant role. Using the Speer & Aubrey (1985) assumption that shallow subtidal areas are momentum sinks, Jay (1991) showed that tidal amplitudes follow a modified Green's law relationship and are proportional to $b_T^{-1/4} b^{-1/4} h^{-1/4}$, where h is depth, b_T is the total width of the estuary, and b is the width of the main channel. Assuming a constant-width channel, a doubling in estuary width b_T produces an approximately 16% decrease in tidal amplitudes, while a halving produces a 19% increase in amplitude. As suggested by Song et al. (2013), the storage effect of tidal flats can therefore be greater than the dissipative effects and can explain the modeled increase in M_2 in the East China Sea. For all these reasons, the effect of wetland reclamation (width changes) must be evaluated on a case-by-case basis.

Choking effect: the tendency of inlets that are small to limit the amount of water that flows into a bay, resulting in small tides

Choking Effects, Constrictions, and Other Bathymetric Considerations

The geometric factors we have focused on—the depth, length, and width of embayments—are only some of the relevant factors that affect long-wave amplitudes and propagation. In particular, the characteristics of the ocean inlet of a bay also affect its tidal properties (e.g., Aretxabaleta et al. 2017). Based on the analysis of Stigebrandt (1980), and assuming frictionally dominated conditions, Hill (1994) defined an inlet choking number $P = (gb^2 H^3 T^2 / C_d L \eta A_e{}^2)^{1/2}$, where L, b, and H are the length, width, and depth of the inlet, respectively; A_e is the embayment surface area; T is the long-wave (e.g., tidal) period; C_d is the drag coefficient (roughness); and η is the long-wave amplitude (Stigebrandt 1980; see also MacMahan et al. 2014). For small values of P (approximately $P \ll 5$ in the idealized model of Hill 1994), the inlet becomes choked, and long-wave amplitudes strongly decrease within the embayment; effectively, the inlet acts as a filter that damps short-period waves. By contrast, the inlet geometry becomes less important for large values of P (e.g., $P \gg 5$; Hill 1994). Hence, any changes to inlet width or depth (e.g., due to jetties and/or dredging) or embayment area (e.g., due to landfill) may alter the magnitude of induced attenuation, with a response that depends on long-wave properties such as amplitude and period.

Infrastructure improvements and erosion/deposition of sediment have the potential to change inlet choking. For example, Araújo et al. (2008) detailed how the construction of an inlet in the early 1800s and continued deepening amplified the tidal range in a Portuguese lagoon, while increased lagoon area led to a decreased tidal range. Furthermore, a numerical model showed that an increase in subtidal area (due to salt marsh erosion) decreased the M_2 tide in a New Jersey back-barrier estuary by 0.09 m (20%) (Donatelli et al. 2018); effectively, the choking number decreased. The construction of the Yangshan Deep-Water Harbor in Hangzhou Bay, China, decreased the width of the inlet, producing a reduction in tidal amplitudes (Guo et al. 2018); however, over time, scouring of the channel is reducing the choking effect. By contrast, Rusdiansyah et al. (2018) showed that building a seawall would slightly increase the tidal range in Jakarta due to the tidal choking effect. A long-term trend of 0.22 mm/y in the M_2 constituent in Venice, Italy, since 1940 (Ferrarin et al. 2015) is attributed in part to morphological changes at the inlet. Complex resonance processes can also occur, particularly when there are two or more inlets (Aretxabaleta et al. 2017).

Effects of Sea-Level Rise on Tides

Multiple modeling studies have numerically examined the possible effects of sea-level rise on tides, using various sea-level rise scenarios and either rigid (unchanging) land boundaries or soft boundaries that allow increased flooding. The results are often strongly dependent on such modeling choices. Within San Francisco Bay, 1 m of sea-level rise amplified tides when the shoreline was

Amphidrome: a location of zero amplitude around which a tidal wave rotates in the ocean and large basins, such as the North Sea

kept rigid but decreased tides if flooding was allowed (Holleman & Stacey 2014). A model of the effects of sea-level rise with enhanced flooding found slight decreases in the K_1 constituent of the Gulf of Carpentaria, Australia (Harker et al. 2019). Similarly, in the Ems estuary, Ensing et al. (2015) predicted that an increase in tidal amplitudes induced by sea-level rise would be lessened if overland flooding occurred. Tides in a Delaware estuary with fixed boundaries may increase with sea-level rise due to increased convergence, but may decrease if overland flooding occurs (Hall et al. 2013, Lee et al. 2017, Ross et al. 2017). Tides increased differently within various bays in the Gulf of Mexico for different sea-level rise scenarios (Passeri et al. 2016), in ways related to the projected change in inlet area (i.e., the choking effect discussed above).

Possible other reasons for variable responses to sea-level rise include the mass-balance, frictional, and reflection effects discussed above (e.g., examples 1–3). Regional models are also affected by amphidrome movement. Pelling et al. (2013b) found that sea-level rise increased tidal amplitudes in some portions of the Bohai Sea but not others, with some locations seeing a much greater increase when flooding was allowed. Y.F. Li et al. (2016) found similar results but of a smaller magnitude. Pickering et al. (2012) showed that sea-level rise would both increase and decrease tides in the North Sea, in part due to amphidrome movement (see also Haigh et al. 2019).

Tides within the Chesapeake Bay and its multiple sub-estuaries show a variety of responses to sea-level rise, with results depending on both estuary characteristics and model assumptions. Consistent with the analytical results presented here, Du et al. (2018) showed that the length and convergence of an estuary helps determine the extent to which tides will be amplified, with tidal range in some locations predicted to double while others remain relatively stationary. Lee et al. (2017) and Du et al. (2018) showed that, if significant floodplain inundation is allowed, tidal range decreases in many locations. When a hard coastline with no overland flooding is used, tidal range is modeled to increase almost everywhere except at the mouth of the Chesapeake Bay, where movement of the amphidrome induced by sea-level rise reduces tidal range (Lee et al. 2017, Ross et al. 2017). These results are consistent with observations of decreasing tidal range in Norfolk, Virginia (**Figure 2**).

The model results for the Chesapeake Bay, while consistent with one another and with observations in some locations, also highlight the challenges in modeling future conditions. For example, all three studies predicted that tides in Washington, DC, will increase with sea-level rise when a fixed coastline is used, in marked contrast to the 9% decrease observed since the 1850s (compare **Figure 2** with Lee et al. 2017, Ross et al. 2017, and Du et al. 2018). While this does not necessarily invalidate model projections, we note that tides are affected by many factors besides sea-level rise, including morphodynamic processes (e.g., Wang et al. 2014), structures such as bridges and pile dikes, river flow (e.g., Moftakhari et al. 2013), and wetland reclamation or restoration. To better model the future, we suggest that it is necessary to better reproduce past trends in tides and fully account for land use, infrastructure, and river flow changes. An emerging strategy is to validate retrospective models with data found in archives (see, e.g., de Jonge et al. 2014, Talke & Jay 2017, Jalon-Rojas et al. 2018, Helaire et al. 2019, Ralston et al. 2019) as a way of better understanding system trajectory and sensitivities.

Flood Hazard

As sea-level rises, the superposition of tides and storm surge onto a higher baseline of water levels will increase flood hazard (e.g., Kemp & Horton 2013). Moreover, tides, surge, and waves may respond nonlinearly to increased depths, sometimes increasing extreme flood risk and infrastructure requirements (Arns et al. 2017). Recent decades have also seen a precipitous increase in nuisance or sunny-day flooding, defined as flooding caused by tides during periods of relatively

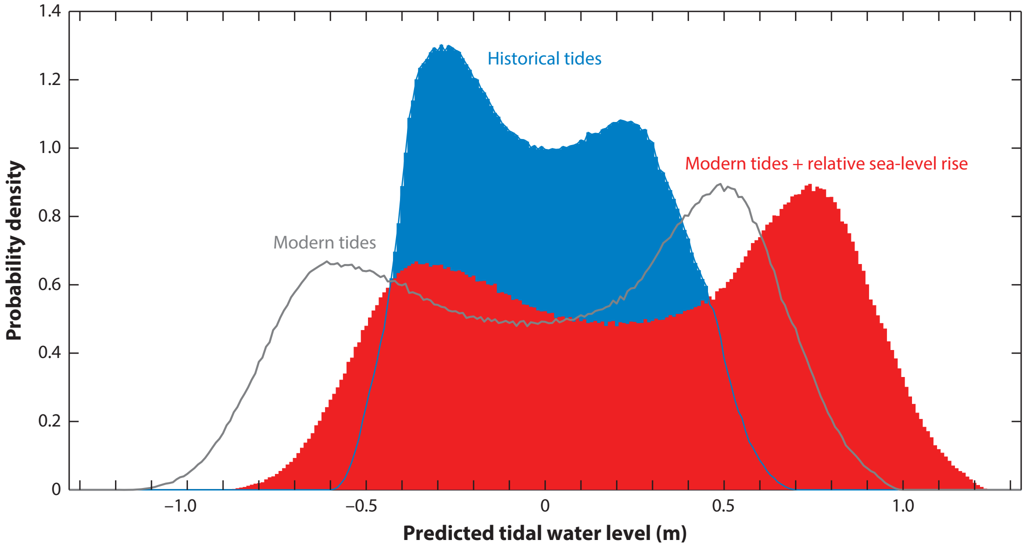

Figure 6

Distribution of predicted hourly tidal elevations in Wilmington, North Carolina, over an 18.61-year nodal cycle based on historical (1887) and modern (2017) hourly records. The gray curve indicates the modern distribution of predicted tidal water levels if no relative sea-level rise had occurred, while the red curve includes an estimated ~0.25 m of sea-level rise since 1910, based on the NOAA trend line from 1935 to 2018 (e.g., Sweet et al. 2017). The predicted water levels and nodal corrections were made using T-TIDE (Pawlowicz et al. 2002). The data are described in Familkhalili & Talke (2016).

small atmospheric forcing (Sweet & Park 2014, Moftakhari et al. 2015, Ray & Foster 2016). These relatively more frequent, smaller floods may prove to be more costly at some locations than large, infrequent extreme events (Moftakhari et al. 2017). Sea-level rise inherently produces nonlinear increases in the frequency of nuisance flooding, not only because the rate of sea-level rise appears to be accelerating (e.g., Dangendorf et al. 2017) but also because the probability distribution of high tide elevations is nonlinear. Hence, each incremental increase in sea level can produce a large (and variable) increase in the number of events above a flood datum (e.g., Sweet & Park 2014, Moftakhari et al. 2015, Burgos et al. 2018).

Long-term changes to tidal amplitudes (e.g., **Figures 2** and **4**) also influence the probability of nuisance flooding, as illustrated by considering the case of Wilmington, North Carolina (**Figure 6**). Compared with a century ago, the distribution of tidal water levels is quite different. Increases to tidal constituents such as M_2 (Familkhalili & Talke 2016) have caused the modern probability distribution to spread out, with lower peaks (compare the gray curve with the blue curve in **Figure 6**). Consistent with other observations from tidal rivers (e.g., Jay et al. 2011), the low-water side of the distribution is more affected than high waters, which can result from the changing amplitude and relative phase of overtides and other constituents (Friedrichs & Aubrey 1988). Nonetheless, considering only tide changes (gray curve versus blue curve in **Figure 6**), the probability distribution of high waters has shifted upward by 0.2–0.25 m. This is the same order of magnitude as local sea-level rise, which has increased by approximately 0.25 m in the last century at Wilmington (Sweet et al. 2017). Putting the effect of sea-level rise and tide change together (red curve in **Figure 6**), we find that the probability of nuisance flooding has greatly increased in Wilmington.

Both nuisance flooding and lower-probability, higher-impact events are inherently variable on seasonal, annual, and decadal timescales due to variations in tidal forcing. Multiple studies show that the probability of tidal flooding that occurs 1–10 times a year is strongly influenced by the 18.61-year nodal cycle and the 8.85-year cycle of lunar perigee (Woodworth & Blackman 2004, Menendez & Woodworth 2010, Haigh et al. 2011, Merrifield et al. 2013, Ray & Foster 2016, Rueda et al. 2017). Talke et al. (2018) showed that nodal variability also affected the 10- and 100-year return-period flood magnitude in Boston. Seasonal modulations of tidal amplitudes on the order of 5–10% that are caused by stratification and/or frictional effects may also be important regionally (e.g., Gräwe et al. 2014, Müller et al. 2014).

The landscape and depth changes that affect tides also affect the propagation and amplitudes of storm surge within estuaries (Familkhalili & Talke 2016) and coastal wetlands (Bilskie et al. 2014), since both are long waves with a wavelength that is large compared with depth. Familkhalili & Talke (2016) found that the worst-case-scenario storm surge (a category 5 hurricane) increased in the Cape Fear estuary on the order of 1–2 m due to channel deepening over the past century, consistent with an increase in tidal amplitudes. Dynamically, many of the parameters that influence tide propagation also affect storm surge waves (R. Familkhalili, S.A. Talke & D.A. Jay, manuscript in review). For example, a slow-moving storm with a long timescale is dissipated less within an estuary or harbor than a fast-moving storm (Orton et al. 2015), much as a low-frequency tide wave is dissipated less (see Equation 4). Similarly, increased depth (e.g., from dredging) reduces the damping on both tides and storm surge (e.g., Ralston et al. 2019), producing a spatially variable increase in amplitude (e.g., Equation 5; S.A. Talke, R. Familkhalili & D.A. Jay, manuscript in preparation).

To first order, a simple rule therefore applies: Regions that exhibit large changes to tides are also likely sensitive to altered storm surge amplitudes (Familkhalili & Talke 2016, Ralston et al. 2019). However, more work is needed to elucidate the compound effects of local wind and river flow on storm surge and how they change with sea-level rise and channel deepening (S.A. Talke, R. Familkhalili & D.A. Jay, manuscript in preparation). Moreover, there is a need to better understand the influence of storm track, storm size, and propagation speed (e.g., Orton et al. 2016) and how tides and surge interact nonlinearly. Nonetheless, we suggest that the tools of tide analysis discussed here provide a template for understanding how surge amplitudes within estuaries will be transformed by sea-level rise.

Ecological Effects

The intertidal zone is marked by significant vertical gradients in flora and fauna both on the rocky shoreline and within estuaries and tidal rivers. Pugh (1987) pointed out that the daily pattern of tide motion, set by the summation of multiple tidal constituents, strongly influences the amount of time intertidal fauna are exposed to desiccation. Similarly, Jay et al. (2016) showed that tides (along with river flow) strongly influence the amount of time a wetland is inundated during the growing season, which correlates strongly with the flora present and habitat function. Within this context, long-term changes to tides—whether astronomical or caused by infrastructure, river flow changes, and sea-level rise—may affect vertical zonation and ecological functioning in ways that have been little explored (but see also Kukulka & Jay 2003b).

Tides, as shown in this review, are often some of the only oceanographic data that extend back to time periods before twentieth-century dredging and infrastructure development. The evolution of tide properties therefore implicitly provides a history of environmental change (Reidy 2008). Where tides have shifted, transport processes, water quality, and ecologically important system properties often have as well. For example, multiple studies have shown that changes to tidal amplitudes and tidal asymmetry induced by channel deepening contributed to an upstream movement and amplification of the Ems turbidity maximum (Chernetsky et al. 2010, de Jonge et al. 2014, van Maren et al. 2015, Dijkstra et al. 2019), leading to the formation of more than

30 km of fluid mud and hypoxic (low-oxygen) conditions (Talke et al. 2009a,b). Similarly, the loss of habitat is often associated with changed tides (e.g., Donatelli et al. 2018). Therefore, we suggest that tidal evolution is a hydrographic marker that may cause—but also reflect—ecological change.

CONCLUSIONS

A review of the literature shows that nonastronomical, temporal variability in estuarine tide properties is common but varies with location and reacts to changes in system geometry, friction, and boundary forcing (e.g., river flow). Tide evolution is often most prominent in highly frictional, shallow systems, and the largest changes are often noted in systems where dredging has greatly increased depths. Changes are also associated with regions that contain strong spatial gradients in tide properties and systems with reflective tides. Alterations in system convergence also affect amplification. An example of many of these changes is the landward part of the Ems estuary, where the tidal range has been amplified by more than a factor of five since the late 1800s.

In the future, sea-level rise may increasingly play a large role in the evolution of tides, particularly if high-end scenarios of sea-level rise occur. Based on this review, it is clear that sea-level rise affects tides primarily through depth changes that alter frictional, convergence, and reflection/resonance properties, but also potentially through other associated geometric factors, such as changes in basin width, length, and tidal flat area, or inlet cross-sectional area. The projected extent of future flooding is often quite sensitive to model details and depends in part on the engineered response (or lack thereof) to sea-level rise (e.g., Pelling & Green 2013, Pelling et al. 2013b, Lee et al. 2017). Thus, it remains unclear how much tidal evolution will occur. Since small- and large-scale infrastructure (e.g., bridges and dikes) have historically altered estuary dissipation and tidal dynamics, the aggregate system-scale effect of human interventions on tides and flood risk needs to be assessed (Vellinga et al. 2014). Better projection of future changes to tides will require an improved understanding of the past, through retrospective modeling validated by archival data.

The outsized influence of historical channel deepening (and other environmental changes) on the amplitudes of both tide and storm surge in some estuaries means that it may sometimes be feasible to reverse undesirable outcomes, thereby mitigating some of the future effects of climate change. For example, Orton et al. (2015) suggested that shallowing Jamaica Bay in New York Harbor and returning to historical depths would provide protection against future sea-level rise, by lowering not only the tides but also the storm surge magnitude of large hurricane events. Similarly, C. Li et al. (2016) showed that creating retention basins in the Ems estuary (if they were placed correctly) would reduce tidal amplitudes and mitigate against high sediment concentration. However, since changes in tidal amplitudes also affect velocities, erosion, residence time, and scalar transport processes (Chant et al. 2018), careful assessment of costs and benefit is needed.

Many myths and folk tales describe the inevitability, the imperturbable nature, of tides. King Canute could not command the tide; London Bridge was falling down, despite any and all efforts to shore it up; and, of course, time and tide wait for no one (Aldersey-Williams 2016, White 2017). Such old folk wisdom is being revised; while humans do not command the tide, they certainly influence tides locally, on a global scale that reflects our global impact on the coastal zone. Past system interventions and infrastructure development have largely occurred without regard to long-term, often incremental tidal evolution, or the cascade of adverse effects that can be associated with such trends. Sea-level rise may compound the effects of tidal evolution—for example, through nonlinear amplification of flood risk (e.g., Arns et al. 2017). However, a better understanding of tide dynamics and tide evolution can lead to better future management of coastal systems for both humans and ecology. What narrative will be told by future generations, and how will this story be reflected in the tides?

DISCLOSURE STATEMENT

The authors are not aware of any affiliations, memberships, funding, or financial holdings that might be perceived as affecting the objectivity of this review.

ACKNOWLEDGMENTS

S.A.T. was funded by NSF CAREER award 1455350. We thank Henk Schuttelaars and an anonymous reviewer for helpful comments on an earlier version of this review. We also thank Philip Orton, Ivan Haigh, Richard Ray, Ed Zaron, Huib de Swart, and many others over the years for helpful discussions regarding tides.

LITERATURE CITED

Aiken CM. 2008. Barotropic tides of the Chilean Inland Sea and their sensitivity to basin geometry. *J. Geophys. Res.* 113:C08024

Aldersey-Williams H. 2016. *The Tide: The Science and Stories Behind the Greatest Force on Earth*. New York: Norton

Amin M. 1983. On perturbations of harmonic constants in the Thames Estuary. *Geophys. J. Int.* 73:587–603

Araújo IB, Dias JM, Pugh DT. 2008. Model simulations of tidal changes in a coastal lagoon, the Ria de Aveiro (Portugal). *Cont. Shelf Res.* 28:1010–25

Arbic BK, Garrett C. 2010. A coupled oscillator model of shelf and ocean tides. *Cont. Shelf Res.* 30:564–74

Arbic BK, Karsten RH, Garrett C. 2009. On tidal resonance in the global ocean and the back-effect of coastal tides upon open-ocean tides. *Atmos.-Ocean* 47:239–66

Aretxabaleta AL, Ganju NK, Butman B, Signell RP. 2017. Observations and a linear model of water level in an interconnected inlet-bay system. *J. Geophys. Res. Oceans* 122:2760–80

Arns A, Dangendorf S, Jensen J, Talke S, Bender J, Pattiaratchi C. 2017. Sea-level rise induced amplification of coastal protection design heights. *Sci. Rep.* 7:40171

Barnard PL, Erikson LH, Kvitek RG. 2011. Small-scale sediment transport patterns and bedform morphodynamics: new insights from high-resolution multibeam bathymetry. *Geo-Mar. Lett.* 31:227–36

Best J. 2005. The fluid dynamics of river dunes: a review and some future research directions. *J. Geophys. Res.* 110:F04S02

Bilskie MV, Hagen SC, Medeiros SC, Passeri DL. 2014. Dynamics of sea level rise and coastal flooding on a changing landscape. *Geophys. Res. Lett.* 41:927–34

Blanchard J. 1941. The history of electrical resonance. *Bell Syst. Tech. J.* 20:415–33

Burgos AG, Hamlington BD, Thompson PR, Ray RD. 2018. Future nuisance flooding in Norfolk, VA, from astronomical tides and annual to decadal internal climate variability. *Geophys. Res. Lett.* 45:12432–39

Buschman FA, Hoitink AJF, van der Vegt M, Hoekstra H. 2009. Subtidal water level variation controlled by river flow and tides. *Water Resour. Res.* 45:W10420

Cai H, Savenije HHG, Tofflon M. 2012a. A new analytical framework for assessing the effect of sea-level rise and dredging on tidal damping in estuaries. *J. Geophys. Res.* 117:C09023

Cai H, Savenije HHG, Toffolon M. 2014. Linking the river to the estuary: influence of river discharge on tidal damping. *Hydrol. Earth Syst. Sci.* 18:287–304

Cai H, Savenije HHG, Yang Q, Suying O, Yaping L. 2012b. Influence of river discharge and dredging on tidal wave propagation: Modaomen Estuary case. *J. Hydraul. Eng.* 138:885–96

Cartwright DE. 1972. Secular changes in the oceanic tides at Brest, 1711–1936. *Geophys. J. Int.* 30:433–49

Cartwright DE, Tayler RJ. 1971. New computations of the tide-generating potential. *Geophys. J. R. Astron. Soc.* 23:45–74

Case WB, Swanson MA. 1990. The pumping of a swing from the seated position. *Am. J. Phys.* 58:463–67

Chant RJ, Sommerfeld CK, Talke SA. 2018. Impact of channel deepening on tidal and gravitational circulation in a highly engineered estuarine basin. *Estuaries Coasts* 41:1587–600

Chernetsky AS, Schuttelaars HM, Talke SA. 2010. The effect of tidal asymmetry and temporal settling lag on sediment trapping in tidal estuaries. *Ocean Dyn.* 60:1219–41

Church JA, White NJ. 2011. Sea-level rise from the late 19th to the early 21st century. *Surv. Geophys.* 32:585–602

Cushman-Roisin B, Naimie CE. 2002. A 3D finite-element model of the Adriatic tides. *J. Mar. Syst.* 37:279–97

Daborn GR, Dadswell MJ. 1988. Natural and anthropogenic changes in the Bay of Fundy – Gulf of Maine – Georges Bank system. In *Natural and Man-Made Hazards*, ed. MI El-Sabh, TS Murty, pp. 547–60. Dordrecht, Neth.: Springer

Dahl TE, Stedman SM. 2013. *Status and trends of wetlands in the coastal watersheds of the Conterminous United States: 2004 to 2009*. Rep., US Fish Wildl. Serv., US Dep. Interior, Washington, DC, and Natl. Mar. Fish. Serv., Natl. Ocean. Atmos. Adm., Silver Spring, MD

Dangendorf S, Marcos M, Wöppelmann G, Conrad CP, Frederikse T, Riva R. 2017. Reassessment of 20th century global mean sea level rise. *PNAS* 114:5946–51

Danielson S, Curchitser E, Hedstrom K, Weingartner T, Stabeno P. 2011. On ocean and sea ice modes of variability in the Bering Sea. *J. Geophys. Res.* 116:C12034

de Jonge VN, Schuttelaars HM, van Beusekom JMM, Talke SA, de Swart HE. 2014. The influence of channel deepening on estuarine turbidity dynamics, as exemplified by the Ems estuary. *Estuar. Coast. Shelf Sci.* 139:46–59

Devlin AT, Jay DA, Talke SA, Zaron E. 2014. Can tidal perturbations associated with sea level variations in the western Pacific Ocean be used to understand future effects of tidal evolution? *Ocean Dyn*. 64:1093–120

Devlin AT, Jay DA, Zaron ED, Talke SA, Pan J, Lin H. 2017. Tidal variability related to sea level variability in the Pacific Ocean. *J. Geophys. Res. Oceans* 122:8445–63

Devlin AT, Zaron ED, Jay DA, Talke SA, Pan J. 2018. Seasonality of tides in Southeast Asian waters. *J. Phys. Oceanogr.* 48:1169–90

Díez-Minguito M, Baquerizo A, Ortega-Sanchez M, Navarro G, Losada M. 2012. Tide transformation in the Guadalquivir estuary (SW Spain) and process-based zonation. *J. Geophys. Res.* 117:C03019

Dijkstra YM, Brouwer RL, Schuttelaars HM, Schramkowski GP. 2017. The iFlow Modelling Framework v2.4. A modular idealized process-based model for flow and transport in estuaries. *Geosci. Model Develop.* 10:2691–713

Dijkstra YM, Schuttelaars HM, Schramkowski GP, Brouwer RL. 2019. Modeling the transition to high sediment concentrations as a response to channel deepening in the Ems River Estuary. *J. Geophys. Res. Oceans* 124:1578–94

DiLorenzo JL, Huang P, Thatcher ML, Najarian TO. 1993. Dredging impacts on Delaware Estuary tides. In *Estuarine and Coastal Modeling III: Proceedings of the 3rd International Conference*, ed. ML Spaulding, K Bedford, A Blumberg, R Cheng, C Swanson, pp. 86–104. Reston, VA: Am. Soc. Civil Eng.

Donatelli C, Ganju NK, Zhang X, Fagherazzi S, Leonardi N. 2018. Salt marsh loss affects tides and the sediment budget in shallow bays. *J. Geophys. Res. Earth Surface* 123:2647–62

Doodson AT. 1921. The harmonic development of the tide-generating potential. *Proc. R. Soc. A* 100:306–28

Doodson AT. 1924. Perturbations of harmonic tidal constants. *Proc. R. Soc. A* 106:513–26

Dronkers JJ. 1964. *Tidal Computations in Rivers and Coastal Waters*. New York: Wiley

Du J, Shen J, Zhang YJ, Ye F, Liu Z, et al. 2018. Tidal response to sea-level rise in different types of estuaries: the importance of length, bathymetry, and geometry. *Geophys. Res. Lett.* 45:227–35

Duff G. 1970. Tidal resonance and tidal barriers in the Bay of Fundy system. *J. Fish. Res. Board Can.* 27:1701–28

Ensing H, de Swart HE, Henk HM, Schuttelaars M. 2015. Sensitivity of tidal motion in well-mixed estuaries to cross-sectional shape, deepening, and sea level rise: an analytical study. *Ocean Dyn*. 65:933–50

Familkhalili R, Talke SA. 2016. The effect of channel deepening on storm surge: a case study of Wilmington, NC. *Geophys. Res. Lett.* 43:9138–47

Feng X, Tsimplis MN, Woodworth PL. 2015. Nodal variations and long-term changes in the main tides on the coasts of China. *J. Geophys. Res. Oceans* 120:1215–32

Ferrarin C, Maicu F, Umgiesser G. 2017. The effect of lagoons on Adriatic Sea tidal dynamics. *Ocean Model.* 119:57–71

Ferrarin C, Tomasin A, Bajo M, Petrizzo A, Umgiesser G. 2015. Tidal changes in a heavily modified coastal wetland. *Cont. Shelf Res.* 101:22–33

Flick RE, Murray JF, Ewing LC. 2003. Trends in United States tidal datum statistics and tide range. *J. Waterway Port Coast. Ocean Eng.* 129:155–64

Fong S, Heaps N. 1978. *Note on the quarter-wave tidal resonance in the Bristol Channel*. Rep. 63, Inst. Oceanogr. Sci., Surrey, UK

Foreman MGG. 1977. *Manual for tidal currents analysis and prediction*. Pac. Mar. Sci. Rep. 77-10, Inst. Ocean Sci., Sidney, BC, Can.

Foreman MGG, Henry RF. 1989. The harmonic analysis of tidal model time series. *Adv. Water Resour.* 12:109–20

Foreman MGG, Henry RF, Walters RA, Ballantyne VA. 1993. A finite element model for tides and resonance along the north coast of British Columbia. *J. Geophys. Res.* 98:2509–31

Friedrichs CT. 2010. Barotropic tides in channelized estuaries. In *Contemporary Issues in Estuarine Physics*, ed. A Valle-Levinson, pp. 27–61. Cambridge, UK: Cambridge Univ. Press

Friedrichs CT, Aubrey DG. 1988. Non-linear tidal distortion in shallow well-mixed estuaries: a synthesis. *Estuar. Coast. Shelf Sci.* 27:521–45

Friedrichs CT, Aubrey DG. 1994. Tidal propagation in strongly convergent channels. *J. Geophys. Res.* 99:3321–36

Gallo MN, Vinzon SB. 2005. Generation of overtides and compound tides in Amazon estuary. *Ocean Dyn.* 55:441–48

Gao GD, Wang XH, Bao XW. 2014. Land reclamation and its impact on tidal dynamics in Jiaozhou Bay, Qingdao, China. *Estuar. Coast. Shelf Sci.* 151:285–94

Garel E, Cai H. 2018. Effects of tidal-forcing variations on tidal properties along a narrow convergent estuary. *Estuaries Coasts* 41:1924–42

Garrett CJR. 1972. Tidal resonance in the Bay of Fundy and Gulf of Maine. *Nature* 238:441–43

Garrett CJR, Keeley JR, Greenberg DA. 1978. Tidal mixing versus thermal stratification in the Bay of Fundy and Gulf of Maine. *Atmos.-Ocean* 16:403–23

Giese BS, Jay DA. 1989. Modelling tidal energetics of the Columbia River Estuary. *Estuar. Coast. Shelf Sci.* 29:549–71

Gilbert GK. 1917. *Hydraulic-mining débris in the Sierra Nevada*. Prof. Pap. 105, US Geol. Surv., Washington, DC

Godin G. 1986. The use of nodal corrections in the calculation of harmonic constants. *Int. Hydrogr. Rev.* 63:143–62

Godin G. 1991. Compact approximations to the bottom friction term, for the study of tides propagating in channels. *Cont. Shelf Res.* 11:579–89

Godin G. 1993. On tidal resonance. *Cont. Shelf Res.* 13:89–107

Godin G. 1995. Rapid evolution of the tide in the Bay of Fundy. *Cont. Shelf Res.* 15:369–72

Godin G. 1999. The propagation of tides up rivers with special considerations on the upper Saint Lawrence River. *Estuar. Coast. Shelf Sci.* 48:307–24

Gräwe U, Burchard H, Müller M, Schuttelaars HM. 2014. Seasonal variability in M_2 and M_4 tidal constituents and its implications for the coastal residual sediment transport. *Geophys. Res. Lett.* 41:5563–70

Green G. 1837. On the motion of waves in a variable canal of small depth and width. *Trans. Camb. Philos. Soc.* 6:457–62

Greenberg DA, Blanchard W, Smith B, Barrow E. 2012. Climate change, mean sea level and high tides in the Bay of Fundy. *Atmos.-Ocean* 50:261–76

Guo L, van der Wegen M, Jay DA, Matte P, Wang ZB, et al. 2015. River-tide dynamics: exploration of nonstationary and nonlinear tidal behavior in the Yangtze River estuary. *J. Geophys. Res. Oceans* 120:3499–521

Guo W, Wang XH, Ding P, Ge J, Song D. 2018. A system shift in tidal choking due to the construction of Yangshan Harbour, Shanghai, China. *Estuar. Coast. Shelf Sci.* 206:49–60

Haigh ID, Eliot M, Pattiaratchi C. 2011. Global influences of the 18.61 year nodal cycle and 8.85 year cycle of lunar perigee on high tidal levels. *J. Geophys. Res. Oceans* 116:C06025

Haigh ID, Pickering MD, Green JAM, Arbic BK, Arns A, et al. 2019. The tides they are a changin'. *Rev. Geophys.* In press

Hall GF, Hill DF, Horton BP, Engelhart SE, Peltier WR. 2013. A high-resolution study of tides in the Delaware Bay: past conditions and future scenarios. *Geophys. Res. Lett.* 40:338–42

Hallegatte S, Green C, Nicholls RJ, Corfee-Morlot J. 2013. Future flood losses in major coastal cities. *Nat. Clim. Change* 3:802–6

Harker A, Green JAM, Schindelegger M, Wilmes S-B. 2019. The impact of sea-level rise on tidal characteristics around Australia. *Ocean Sci*. 15:147–59

Hay CC, Morrow E, Kopp RE, Mitrovica JX. 2015. Probabilistic reanalysis of twentieth-century sea-level rise. *Nature* 517:481–84

Helaire LT, Talke SA, Jay DA, Mahedy D. 2019. Historical changes in lower Columbia River and Estuary floods: a numerical study. J. Geophys. Res. Oceans. In press. **https://doi.org/10.1029/2019JC015055**

Hill AE. 1994. Fortnightly tides in a lagoon with variable choking. *Estuar. Coast. Shelf Sci.* 38:423–34

Hill DF. 2016. Spatial and temporal variability in tidal range: evidence, causes, and effects. *Curr. Clim. Change Rep.* 2:232–41

Hinkel J, Lincke D, Vafeidis AT, Perrette M, Nicholls RJ, et al. 2014. Coastal flood damage and adaptation costs under 21st century sea-level rise. *PNAS* 111:3292–97

Hoitink AJF, Jay DA. 2016. Tidal river dynamics: implications for deltas. *Rev. Geophys.* 54:240–72

Hollebrandse FAP. 2005. *Temporal development of the tidal range in the southern North Sea*. MS Thesis, Delft Univ. Technol., Delft, Neth.

Holleman RC, Stacey MT. 2014. Coupling of sea level rise, tidal amplification, and inundation. *J. Phys. Oceanogr.* 44:1439–55

Idier D, Paris F, Cozannet GL, Boulahya F, Dumas F. 2017. Sea-level rise impacts on the tides of the European Shelf. *Cont. Shelf Res.* 137:56–71

IHO (Int. Hydrogr. Organ.). 1994. *Hydrographic Dictionary: Part I*, *Volume I*, *English*. Spec. Publ. 32. Monaco: IHO. 5th ed.

Jalon-Rojas I, Sottolichio A, Hanquiez V, Fort A, Schmidt S. 2018. To what extent multidecadal changes in morphology and fluvial discharge impact tide in a convergent (turbid) tidal river. *J. Geophys. Res. Oceans* 123:3241–58

Jay DA. 1991. Green's law revisited: tidal long wave propagation in channels with strong topography. *J. Geophys. Res.* 96:20585–98

Jay DA. 2009. Evolution of tidal amplitudes in the eastern Pacific Ocean. *Geophys. Res. Lett.* 36:L04603

Jay DA, Giese BS, Sherwood CR. 1990. Energetics and sedimentary processes in the Columbia River Estuary. *Prog. Oceanogr.* 25:157–74

Jay DA, Leffler K, Degens S. 2011. Long-term evolution of Columbia River tides. *J. Waterway Port Coast. Ocean Eng.* 137:182–91

Jay DA, Leffler K, Diefenderfer HL, Borde AB. 2015. Tidal-fluvial and estuarine processes in the lower Columbia River: I. Along-channel water level variations, Pacific Ocean to Bonneville Dam. *Estuaries Coasts* 38:415–33

Jay DA, Leffler K, Diefenderfer HL, Borde AB. 2016. Tidal-fluvial and estuarine processes in the lower Columbia River: II. Water level models, floodplain wetland inundation, and system zones. *Estuaries Coasts* 39:1299–324

Jensen J, Mudersbach C. 2007. Zeitliche Änderungen in den Wasserstandszeitreihen an den Deutschen Küsten. *Ber. Dtsch. Landeskd.* 81:99–112

Katavouta A, Thompson KR, Lu Y, Loder JW. 2016. Interaction between the tidal and seasonal variability of the Gulf of Maine and Scotian Shelf region. *J. Phys. Oceanogr.* 46:3279–98

Kemp AC, Hill TD, Bernhardt C, Vane CH, Cahill N, et al. 2017. Relative sea-level trends in New York City during the past ∼1500 years. *Holocene* 27:1169–86

Kemp AC, Horton BP. 2013. Contribution of relative sea-level rise to historical hurricane flooding in New York City. *J. Quat. Sci.* 28:537–41

Kenchington EL, Kenchington TJ, Henry LA, Fuller S, Gonzalez P. 2007. Multi-decadal changes in the megabenthos of the Bay of Fundy: the effects of fishing. *J. Sea Res.* 58:220–40

Kukulka T, Jay DA. 2003a. Impacts of Columbia River discharge on salmonid habitat: 1. A non-stationary fluvial tide model. *J. Geophys. Res.* 108:3293

Kukulka T, Jay DA. 2003b. Impacts of Columbia River discharge on salmonid habitat: 2. Changes in shallow-water habitat. *J. Geophys. Res.* 108:3294
Kvale EP. 2006. The origin of neap-spring tidal cycles. *Mar. Geol.* 235:5–18
Lanzoni S, Seminara G. 1998. On tide propagation in convergent estuaries. *J. Geophys. Res.* 103:30793–812
LeBlond PH. 1978. On tidal propagation in shallow rivers. *J. Geophys. Res. Atmos.* 83:4717–21
Lee SB, Li M, Zhang F. 2017. Impact of sea level rise on tidal range in Chesapeake and Delaware Bays. *J. Geophys. Res. Oceans* 122:3917–38
Li C, Schuttelaars HM, Roos PC, Damveld JH, Gong W, Hulscher SJMH. 2016. Influence of retention basins on tidal dynamics in estuaries: application to the Ems estuary. *Ocean Coast. Manag.* 134:216–25
Li C, Valle-Levinson A. 1999. A two-dimensional analytic tidal model for a narrow estuary of arbitrary lateral depth variation: the intratidal motion. *J. Geophys. Res. Oceans* 104:23525–43
Li L, Guan W, Hu J, Cheng P, Wang XH. 2018. Responses of water environment to tidal flat reduction in Xiangshan Bay: part I hydrodynamics. *Estuar. Coast. Shelf Sci.* 206:14–26
Li YF, Zhang H, Tang C, Zou T, Jiang DJ. 2016. Influence of rising sea level on tidal dynamics in the Bohai Sea. *J. Coast. Res.* Spec. Issue 74:22–31
Liang D, Xia J, Falconer RA, Zhang J. 2014. Study on tidal resonance in Severn Estuary and Bristol Channel. Coast. Eng. J. 56:1450002-1–18
Losada MA, Díez-Minguito M, Reyes-Merlo M. 2017. Tidal-fluvial interaction in the Guadalquivir River Estuary: spatial and frequency-dependent response of currents and water levels. *J. Geophys. Res. Oceans* 122:847–65
MacMahan J, van de Kreeke J, Reniers A, Elgar S, Raubenheimer B, et al. 2014. Fortnightly tides and subtidal motions in a choked inlet. *Estuar. Coast. Shelf Sci.* 150:325–31
Marmer HA. 1922. Tides in the Bay of Fundy. *Geogr. Rev.* 12:195–205
Marmer HA. 1935. *Tides and Currents in New York Harbor*. Washington, DC: Gov. Print. Off.
Matte P, Jay DA, Zaron ED. 2013. Adaptation of classical tidal harmonic analysis to nonstationary tides, with application to river tides. *J. Atmos. Ocean. Technol.* 30:569–89
Matte P, Secretan Y, Morin J. 2014. Temporal and spatial variability of tidal-fluvial dynamics in the St. Lawrence fluvial estuary: an application of nonstationary tidal harmonic analysis. *J. Geophys. Res. Oceans* 119:5724–44
Mawdsley RJ, Haigh ID, Wells NC. 2015. Global secular changes in different tidal high water, low water and range levels. *Earth's Future* 3:66–81
Menendez M, Woodworth PL. 2010. Changes in extreme high water levels based on a quasi-global tide-gauge dataset. *J. Geophys. Res.* 115:C10011
Merrifield MA, Genz AS, Kontoes CP, Marra JJ. 2013. Annual maximum water levels from tide gauges: contributing factors and geographic patterns. *J. Geophys. Res.* 118:2535–46
Miles JW. 1971. Resonant response of harbors: an equivalent-circuit analysis. *J. Fluid Mech.* 46:241–65
Moftakhari HR, AghaKouchak A, Sanders BF, Feldman DL, Sweet W, et al. 2015. Increased nuisance flooding along the coasts of the United States due to sea level rise: past and future. *Geophys. Res. Lett.* 42:9846–52
Moftakhari HR, AghaKouchak A, Sanders BF, Matthew RA. 2017. Cumulative hazard: the case of nuisance flooding. *Earth's Future* 5:214–23
Moftakhari HR, Jay DA, Talke SA. 2016. Estimating river discharge using multiple-tide gauges distributed along a channel. *J. Geophys. Res. Oceans* 121:2078–97
Moftakhari HR, Jay DA, Talke SA, Kukulka T, Bromirski PD. 2013. A novel approach to flow estimation in tidal rivers. *Water Resour. Res.* 49:4817–32
Montgomery DR. 2007. *Dirt: The Erosion of Civilizations*. Berkeley: Univ. Calif. Press
Müller M. 2011. Rapid change in semi-diurnal tides in the North Atlantic since 1980. *Geophys. Res. Lett.* 38:L11602
Müller M. 2012. The influence of changing stratification conditions on barotropic tidal transport and its implications for seasonal and secular changes of tides. *Cont. Shelf Res.* 47:107–18
Müller M, Arbic BK, Mitrovica JX. 2011. Secular trends in ocean tides: observations and model results. *J. Geophys. Res.* 116:C05013

Müller M, Cherniawsky J, Foreman M, von Storch J-S. 2014. Seasonal variation of the M_2 tide. *Ocean Dyn*. 64:159–77

Murray NJ, Clemens RS, Phinn SR, Possingham HP, Fuller RA. 2014. Tracking the rapid loss of tidal wetlands in the Yellow Sea. *Front. Ecol. Environ.* 12:267–72

Naik P, Jay DA. 2011. Distinguishing human and climate impacts on Columbia River: changes in mean flow and sediment transport. *J. Hydrol.* 404:259–77

Nepf H. 1999. Drag, turbulence, and diffusion in flow through emergent vegetation. *Water Resour. Res.* 35:479–89

Neumann B, Vafeidis AT, Zimmermann J, Nicholls RJ. 2015. Future coastal population growth and exposure to sea-level rise and coastal flooding – a global assessment. *PLOS ONE* 10:e0118571

Nicholls RJ, Cazenave A. 2010. Sea-level rise and its impact on coastal zones. *Science* 328:1517–20

Nicholls RJ, Hoozemans FMJ, Marchand M. 1999. Increasing flood risk and wetland losses due to global sea-level rise: regional and global analyses. *Glob. Environ. Change* 9:S69–87

Oey L-Y, Ezer T, Hu C, Muller-Karger FE. 2007. Baroclinic tidal flows and inundation processes in Cook Inlet, Alaska: numerical modeling and satellite observations. *Ocean Dyn*. 57:205–21

Orton PM, Hall TM, Talke SA, Georgas N, Blumberg AF, Vinogradov S. 2016. A validated tropical-extratropical flood hazard assessment for New York Harbor. *J. Geophys. Res.* 121:8904–29

Orton PM, Talke SA, Jay DA, Yin L, Blumberg AF, et al. 2015. Channel shallowing as mitigation of coastal flooding. *J. Mar. Sci. Eng.* 3:654–73

Parker BB. 1991. The relative importance of the various nonlinear mechanisms in a wide range of tidal interactions. In *Tidal Hydrodynamics*, ed. BB Parker, pp. 237–68. New York: Wiley

Passeri DL, Hagen SC, Plant NG, Bilskie MV, Medeiros SC, Alizad K. 2016. Tidal hydrodynamics under future sea level rise and coastal morphology in the Northern Gulf of Mexico. *Earth's Future* 4:159–76

Pawlowicz R, Beardsley B, Lentz S. 2002. Classical tidal harmonics analysis including error estimates in MATLAB using T-TIDE. *Comput. Geosci.* 28:929–37

Pelling HE, Green JAM. 2013. Sea level rise and tidal power plants in the Gulf of Maine. *J. Geophys. Res. Ocean* 118:2863–73

Pelling HE, Green JAM, Ward SL. 2013a. Modelling tides and sea-level rise: to flood or not to flood. *Ocean Model*. 63:21–29

Pelling HE, Uehara K, Green JAM. 2013b. The impact of rapid coastline changes and sea level rise on the tides in the Bohai Sea, China. *J. Geophys. Res. Oceans* 118:3462–72

Pickering MD, Horsburgh KJ, Blundell JR, Hirschi JJ-M, Nicholls RJ, et al. 2017. The impact of future sea-level rise on the global tides. *Cont. Shelf Res.* 142:50–68

Pickering MD, Wells NC, Horsburgh KJ, Green JAM. 2012. The impact on the European Shelf tides by future sea-level rise. *Cont. Shelf Res.* 35:1–15

Prandle D. 1991. Tides in estuaries and embayments (review). In *Tidal Hydrodynamics*, ed. BB Parker, pp. 125–52. New York: Wiley & Sons

Prandle D. 2003. Relationships between tidal dynamics and bathymetry in strongly convergent estuaries. *J. Phys. Oceanogr.* 33:2738–50

Prandle D, Rahman M. 1980. Tidal response in estuaries. *J. Phys. Oceanogr.* 10:1552–73

Pugh DT. 1987. *Tides, Surges and Mean Sea Level*. New York: Wiley & Sons

Ralston DK, Talke SA, Geyer WR, Al'Zubadaei H, Sommerfield CK. 2019. Bigger tides, less flooding: effects of dredging on water level in the Hudson River estuary. *J. Geophys. Res.* 124:196–211

Ray RD. 2006. Secular changes of the M tide in the Gulf of Maine. *Cont. Shelf Res.* 26:422–27

Ray RD. 2009. Secular changes in the solar semidiurnal tide of the western North Atlantic Ocean. *Geophys. Res. Lett.* 36:L02610

Ray RD, Foster G. 2016. Future nuisance flooding at Boston caused by astronomical tides alone. *Earth's Future* 4:578–87

Ray RD, Talke SA. 2019. Nineteenth-century tides in the Gulf of Maine and implications for secular trends. *J. Geophys. Res. Oceans*. In press. **https://doi.org/10.1029/2019JC015277**

Reidy MS. 2008. *Tides of History: Ocean Science and Her Majesty's Navy*. Chicago: Univ. Chicago Press

Rodríguez-Padilla I, Ortiz M. 2017. On the secular changes in the tidal constituents in San Francisco Bay. *J. Geophys. Res. Oceans* 122:7395–406
Ross AC, Najjar RG, Li M, Lee SB, Zhang F, Liu W. 2017. Fingerprints of sea level rise on changing tides in the Chesapeake and Delaware Bays. *J. Geophys. Res. Oceans* 122:8102–25
Rueda A, Vitousek S, Camus P, Tomás A, Espejo A, et al. 2017. A global classification of coastal flood hazard climates associated with large-scale oceanographic forcing. *Sci. Rep.* 7:5038
Rusdiansyah A, Tang Y, He1 Z, Li L, et al. 2018. The impacts of the large-scale hydraulic structures on tidal dynamics in open-type bay: numerical study in Jakarta Bay. *Ocean Dyn*. 68:1141–54
Savenije HHG, Toffolon M, Haas J, Veling EJM. 2008. Analytical description of tidal dynamics in convergent estuaries. *J. Geophys. Res.* 113:C10025
Savenije HHG, Veling EJM. 2005. The relation between tidal damping and wave celerity in estuaries. *J. Geophys. Res.* 110:C04007
Schindelegger M, Green JAM, Wilmes SB, Haigh ID. 2018. Can we model the effect of observed sea level rise on tides? *J. Geophys. Res.* 123:4593–609
Schoellhamer DH. 2011. Sudden clearing of estuarine waters upon crossing the threshold from transport to supply regulation of sediment transport as an erodible sediment pool is depleted: San Francisco Bay, 1999. *Estuaries Coasts* 34:885–99
Schureman P. 1934. *Tides and Currents in Hudson River*. Washington, DC: Gov. Print. Off.
Seasholes NS. 2003. *Gaining Ground: A History of Landmaking in Boston*. Cambridge, MA: MIT Press
Simpson JH, Hunter J. 1974. Fronts in the Irish Sea. *Nature* 250:404–6
Skiba AW, Zeng L, Arbic BK, Müller M, Goodwin WJ. 2013. On the resonance and shelf/open-ocean coupling of the global diurnal tides. *J. Phys. Oceanogr.* 43:1301–24
Song D, Wang XH, Zhu X, Bao X. 2013. Modeling studies of the far-field effects of tidal flat reclamation on tidal dynamics in the East China Seas. *Estuar. Coast. Shelf Sci.* 133:147e160
Speer PE, Aubrey D. 1985. A study of non-linear tidal propagation in shallow inlet/estuarine systems, part II: theory. *Estuar. Coast. Shelf Sci.* 21:206–40
Stigebrandt A. 1980. Some aspects of tidal interaction with fjord constrictions. *Estuar. Coast. Mar. Sci.* 11:151–66
Sweet WV, Kopp RE, Weaver CP, Obeysekera J, Horton RM, et al. 2017. *Global and regional sea level rise scenarios for the United States*. Tech. Rep. 83, Natl. Ocean Serv., Natl. Ocean. Atmos. Adm., Silver Spring, MD
Sweet WV, Park J. 2014. From the extreme to the mean: acceleration and tipping points of coastal inundation from sea level rise. *Earth's Future* 2:579–600
Syvitski JPM, Kettner AJ, Overeem I, Hutton EWH, Hannon MT, Brakenridge GR. 2009. Sinking deltas due to human activities. *Nat. Geosci.* 2:681–86
Talke SA, de Swart HE, de Jonge VN. 2009a. An idealized model and systematic process study of oxygen depletion in highly turbid estuaries. *Estuaries Coasts* 32:602–20
Talke SA, de Swart HE, Schuttelaars HM. 2009b. Feedback between residual circulation and sediment distribution in highly turbid estuaries: an analytical model. *Cont. Shelf Res.* 29:119–35
Talke SA, Horner-Devine AR, Chickadel CC. 2010. Mixing layer dynamics in separated flow over an estuarine sill with variable stratification *J. Geophys. Res.* 115:C09004
Talke SA, Horner-Devine AR, Chickadel CC, Jessup AT. 2013. Turbulent kinetic energy and coherent structures in a tidal river. *J. Geophys. Res.* 118:6965–81
Talke SA, Jay DA. 2013. Nineteenth century North American and Pacific tidal data: lost or just forgotten? *J. Coast. Res.* 291:118–27
Talke SA, Jay DA. 2017. *Archival water-level measurements: recovering historical data to help design for the future*. Civil Works Tech. Ser. Rep. 2017-02, US Army Corps Eng. Portland Dist., Portland, OR
Talke SA, Kemp A, Woodruff J. 2018. Relative sea level, tides, and extreme water levels in Boston (MA) from 1825 to 2018. *J. Geophys. Res.* 123:3895–914
Talke SA, Orton P, Jay DA. 2014. Increasing storm tides in New York Harbor, 1844–2013. *Geophys. Res. Lett.* 41:3149–55

Talke SA, Stacey MT. 2003. The influence of oceanic swell on flows over an estuarine intertidal mudflat in San Francisco Bay. *Estuar. Coast. Shelf Sci.* 58:541–54

Templeton WJ, Jay DA. 2013. Lower Columbia river sand supply and removal: estimates of two sand budget components. *J. Waterway Port Coast. Ocean Eng.* 139:383–92

Tennekes H, Lumley JL. 1990. *A First Course in Turbulence*. Cambridge, MA: MIT Press

Terra GM. 2005. *Non-linear tidal resonance*. PhD Thesis, Univ. Amsterdam, Amsterdam

Toffolon M, Savenije HG. 2011. Revisiting linearized one-dimensional tidal propagation. *J. Geophys. Res.* 116:C07007

van de Ven CP. 1993. *Man-Made Lowlands: History of Water Management and Land Reclamation in the Netherlands*. Utrecht, Neth.: Uitgeverij Matrijs

van Maren DS, Winterwerp JC, Vroom J. 2015. Fine sediment transport into the hyper-turbid lower Ems River: the role of channel deepening and sediment-induced drag reduction. *Ocean Dyn*. 65:589–605

van Rijn LC. 2011. Analytical and numerical analysis of tides and salinities in estuaries; part I: tidal wave propagation in convergent tidal channels. *Ocean Dyn*. 61:1719–41

van Rijn LC, Grasmeijer B, Perk L. 2018. Effect of channel deepening on tidal flow and sediment transport: part I—sandy channels. *Ocean Dyn*. 68:1457

Vellinga NE, Hoitink AJF, van der Vegt M, Zhang W, Hoekstra P. 2014. Human impacts on tides overwhelm the effect of sea level rise on extreme water levels in the Rhine-Meuse delta. *Coast. Eng.* 90:40–50

Wang ZB, Winterwerp JC, He Q. 2014. Interaction between suspended sediment and tidal amplification in the Guadalquivir Estuary. *Ocean Dyn*. 64:1487–98

Webb DJ. 2012. On the shelf resonances of the Gulf of Carpentaria and the Arafura Sea. *Ocean Sci*. 8:733–50

White J. 2017. *Tides: The Science and Spirit of the Ocean*. San Antonio, TX: Trinity Univ. Press

Winterwerp JC, Wang ZB. 2013. Man-induced regime shifts in small estuaries—I: theory. *Ocean Dyn*. 63:1279–92

Winterwerp JC, Wang ZB, van Braeckel A, van Holland G, Kösters F. 2013. Man-induced regime shifts in small estuaries—II: a comparison of rivers. *Ocean Dyn*. 63:1293–306

Wong KC. 1990. Sea level variability in Long Island Sound. *Estuaries* 13:362–72

Woodworth PL. 2010. A survey of recent changes in the main components of the ocean tide. *Cont. Shelf Res.* 30:1680–91

Woodworth PL, Blackman DL. 2004. Evidence for systematic changes in extreme high waters since the mid-1970s. *J. Clim.* 17:1190–97

Zaron ED, Jay DA. 2014. An analysis of secular change in tides at open-ocean sites in the Pacific. *J. Phys. Oceanogr.* 44:1704–26

Zhang W, Ruan X, Zheng J, Zhu Y, Wu H. 2010. Long-term change in tidal dynamics and its cause in the Pearl River Delta, China. *Geomorphology* 120:209–23

Zhang X, Church JA. 2012. Sea level trends, interannual and decadal variability in the Pacific Ocean. *Geophys. Res. Lett.* 39:L21701